Molecular Therapy
Original Article

Extracellular vesicle-transmitted miR-671-5p alleviates lung inflammation and injury by regulating the AAK1/NF-κB axis

Jie Lian,[1,2,3,4] Xinxing Zhu,[1,4] Jiang Du,[1] Beijia Huang,[1] Fengting Zhao,[1] Chunya Ma,[1] Rui Guo,[1] Yangxia Zhang,[1] Longkai Ji,[1] Badrul Hisham Yahaya,[2] and Juntang Lin[1,3]

[1]Henan Joint International Research Laboratory of Stem Cell Medicine, School of Medical Engineering, Xinxiang Medical University, Xinxiang 453003, China; [2]Lung Stem Cells and Gene Therapy Group, Department of Biomedical Sciences, Advanced Medical and Dental Institute (AMDI), Universiti Sains Malaysia, SAINS@Bertam, 13200 Kepala Batas, Penang, Malaysia; [3]Stem Cells and Biotherapy Engineering Research Center of Henan, National Joint Engineering Laboratory of Stem Cells and Biotherapy, School of Life Science and Technology, Xinxiang Medical University, Xinxiang 453003, China

Mesenchymal stem cells regulate remote intercellular signaling communication via their secreted extracellular vesicles. Here, we report that menstrual blood-derived stem cells alleviate acute lung inflammation and injury via their extracellular vesicle-transmitted miR-671-5p. Disruption of this abundantly expressed miR-671-5p dramatically reduced the ameliorative effect of extracellular vesicles released by menstrual blood-derived stem cells on lipopolysaccharide (LPS)-induced pulmonary inflammatory injury. Mechanistically, miR-671-5p directly targets the kinase AAK1 for post-transcriptional degradation. AAK1 is found to positively regulate the activation of nuclear factor κB (NF-κB) signaling by controlling the stability of the inhibitory protein IκBα. This study identifies a potential molecular basis of how extracellular vesicles derived from mesenchymal stem cells improve pulmonary inflammatory injury and highlights the functional importance of the miR-671-5p/AAK1 axis in the progression of pulmonary inflammatory diseases. More importantly, this study provides a promising cell-based approach for the treatment of pulmonary inflammatory disorders through an extracellular vesicle-dependent pathway.

INTRODUCTION

Acute lung injury (ALI), or its clinical manifestation, acute respiratory distress syndrome (ARDS), is an acute and serious inflammatory lung injury with high morbidity and mortality as well as development of multiple organ dysfunction syndrome (MODS).[1] Multiple inflammatory mediators and effectors in cells are involved in this process, which shows cascade inflammation, resulting in acute hypoxic respiratory failure. The major manifestations of refractory hypoxemia and respiratory distress are life threatening. With the ongoing global coronavirus disease 2019 (COVID-19) pandemic, there is a parallel rise in the prevalence of ARDS. Clinical outcomes suggest that the mortality rate in COVID-19-associated ARDS is much higher.[2–4] More importantly, crucial advances in pathophysiology and treatment have been made, but there is still no effective pharmacotherapy based on repairing damaged lung tissues for ALI. Therefore, development of new approaches for the clinical treatment of acute lung inflammation and injury is urgently needed.

Cell therapies using mesenchymal stem cells (MSCs) have emerged for treating various untreatable disorders because of their characteristic of multipotent differentiation, capability to replace damaged cells and tissues and paracrine effects, as well as low immunogenicity.[5] MSCs, derived from multiple sources, can secrete a variety of vascular and tissue cell growth factors to promote the recovery and reconstruction of damaged vascular and alveolar tissues, which can rapidly and significantly improve the prognosis of patients and effectively avoid cytokine storm, providing a new idea for the clinical treatment of ALI.[6,7] To date, numerous clinical trials have been targeting ARDS or COVID-19 worldwide, suggesting that MSC transplantation significantly improves lung injury and inflammation in clinical settings.[8,9] Growing evidence indicates that, in addition to soluble factors, extracellular vesicles (EVs) released by MSCs, acting as vehicles for the cross-talk between cells, may critically facilitate immunoregulation, tissue repair and regeneration, as well as inhibition of excessive inflammatory response.[10–12] EVs, including exosomes and microvesicles, are released by all cell types and contain cell-type-specific

Received 10 September 2022; accepted 29 January 2023;
https://doi.org/10.1016/j.ymthe.2023.01.025.

[4]These authors contributed equally

Correspondence: Xinxing Zhu, Henan Joint International Research Laboratory of Stem Cell Medicine, School of Medical Engineering, Xinxiang Medical University, Xinxiang 453003, China.
E-mail: zhuxinxing0202@163.com
Correspondence: Badrul Hisham Yahaya, Lung Stem Cells and Gene Therapy Group, Department of Biomedical Sciences, Advanced Medical and Dental Institute (AMDI), Universiti Sains Malaysia, SAINS@Bertam, 13200 Kepala Batas, Penang, Malaysia.
E-mail: badrul@usm.my
Correspondence: Juntang Lin, Henan Joint International Research Laboratory of Stem Cell Medicine, School of Medical Engineering, Xinxiang Medical University, Xinxiang 453003, China.
E-mail: linjtlin@126.com

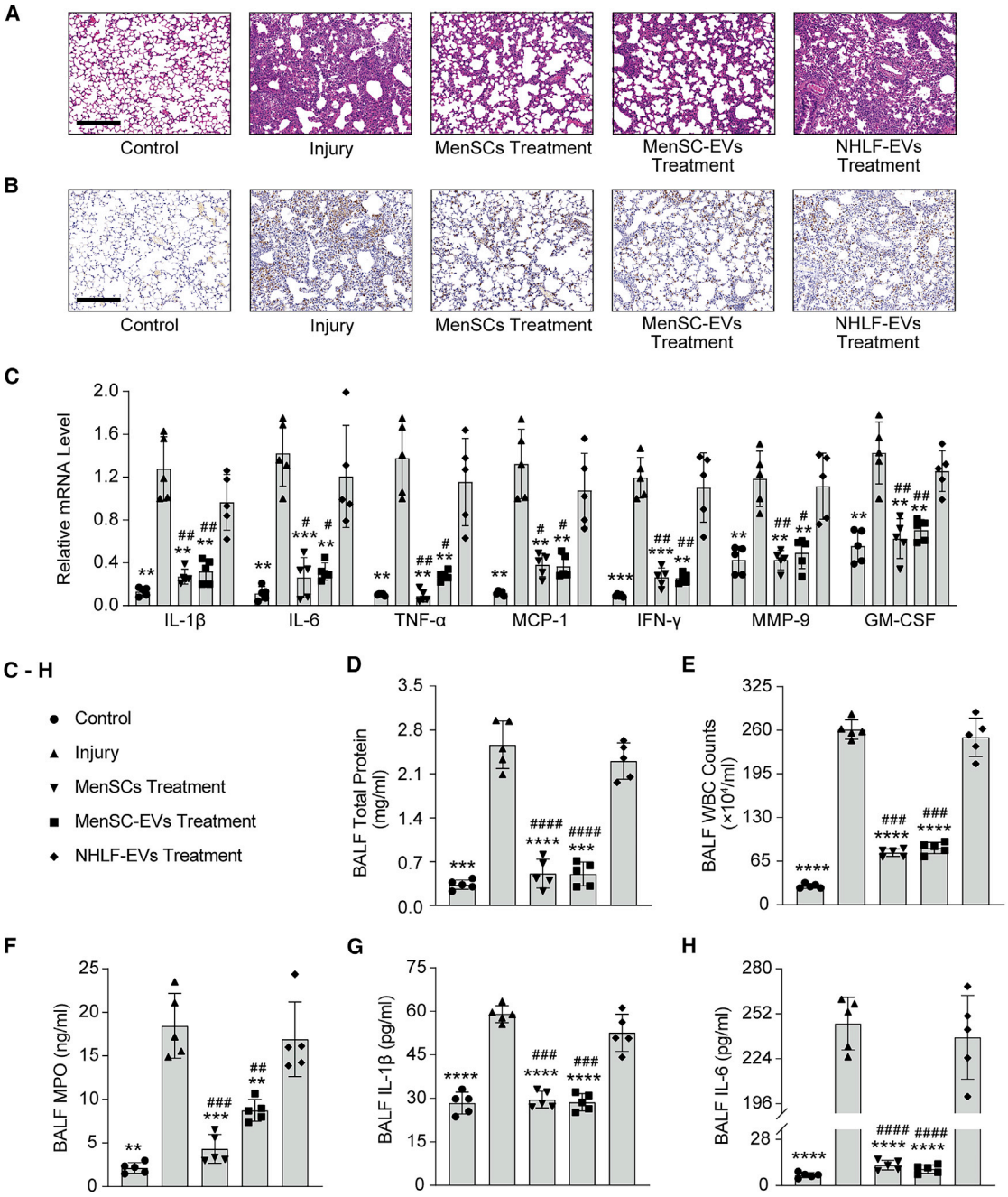

Figure 1. MenSC-EVs, as well as their parent cells, significantly improve LPS-induced ALI mice by i.t. transplantation

(A) Similar to the effect of MenSCs, MenSC-EVs administration dramatically improves ALI in mice, as demonstrated by histological analysis. Lung sections harvested from mice on day 4 post LPS stimulation (4 mg/kg) were subjected to H&E staining. Scale bar, 200 μm. (B) Decreased accumulation of pulmonary macrophages in mice subjected to MenSCs or MenSC-EVs treatment was detected by CD68 IHC staining of lung sections. The mice were sacrificed on day 4 after LPS stimulation (4 mg/kg). Scale bar, 200 μm. (C) Relative mRNA expression of proinflammatory factors in lungs of mice administered MenSCs, MenSC-EVs, or NHLF-EVs in the presence of LPS (4 mg/kg) was detected by qRT-PCR assay. PBS was used as a negative control. (D) Total protein concentration in BALF isolated from mice treated with MenSCs, MenSC-EVs, or NHLF-EVs was measured by BCA to examine the changes in pulmonary vascular and epithelial permeability. The mice were sacrificed on day 4 after LPS stimulation (4 mg/kg). (E and F) WBC counts (E) and MPO activity (F) in BALF isolated from mice treated with MenSCs, MenSC-EVs, or NHLF-EVs was measured to examine the effect of MenSCs or

(legend continued on next page)

and selectively packaged proteins, mRNAs, and small RNAs that are transported stably in circulation and taken up by recipient cells in a process believed to be nonrandom, and delivery of these bioactive molecules may cause functional changes in recipient cells.[13,14] Therefore, MSC-EVs would be one of the most compelling alternatives for cell-free therapy because of their lower risk of allogenic immune rejection, accessible preservation, and higher stability than their parent cells.

MicroRNAs (miRNAs), a class of small non-coding RNAs ~22 nt in length, have been newly identified as critical mediators in modulating diverse inflammatory pathological processes, such as tumorigenesis,[15] pulmonary inflammation,[16–18] and some immunodeficiency diseases.[19–21] Previous studies have shown that extracellular miRNAs can be secreted and transmitted to specific effector cells in an EV-dependent manner for functional modulation, primarily through regulating posttranscriptional gene expression.[22] For example, adipose tissue macrophage-derived exosomes, a crucial component of EVs, can deliver mediator miRNAs to modulate systemic insulin responses through posttranscriptional regulation of PPARγ.[22] Another study also showed bone marrow (BM)-MSC-secreted exosomal miR-182 could be transferred to macrophages by an EV-mediated pathway, promoting M2-oriented polarization to alleviate myocardial ischemia-reperfusion injury by targeting Toll-like receptor 4 (TLR4) degradation.[23] AAK1 (AP2-associated kinase 1), a known CME (Clathrin-mediated endocytosis) enhancer, has been suggested to play a pivotal role in facilitating rabies and hepatitis C virus infection.[24,25] Furthermore, its blockers are being studied as promising therapeutic candidates to disrupt the entry of severe acute respiratory syndrome coronavirus 2 (SARS-CoV-2) into target cells,[26–28] but its intrinsic regulatory mechanism should be investigated more deeply. Numerous inflammatory signaling pathways participate in acute lung inflammation and injury, among which nuclear factor κB (NF-κB) signaling is widely accepted as a leading contributing factor.

Here, we identify that miR-671-5p is required for menstrual blood-derived stem cells (MenSC)-EV-mediated improvement of pulmonary inflammatory injury using the LPS-induced ALI model. miR-671-5p-deficient MenSC-EVs, compared with wild-type MenSC-released EVs, substantially reduced the protective effects on acute lung inflammation and injury, indicating a central role of miR-671-5p in MenSC-based therapy of pulmonary inflammatory disorders. More interestingly, miR-671-5p could directly target the kinase AAK1 for posttranscriptional degradation, and AAK1 is a critical activator of the inflammatory response. Hence, miR-671-5p/AAK1 might be the key cascade responsible for the therapeutic effect of MenSC-EVs on lung inflammation and injury. This study provides new insight into the underlying molecular basis by which MSCs regulate pulmonary inflammatory disorders through their anti-inflammatory properties.

RESULTS

MenSCs, as well as their secreted EVs, dramatically alleviate LPS-induced ALI by intratracheal transplantation

It is well known that MSC-based improvement of multiple inflammatory disorders majorly depends on their paracrine action.[29–33] Thus, we proposed that MenSC-derived EVs, known to mediate intercellular communication via carrying critical regulators, such as miRNAs and some other protein factors, are likely to participate in MenSC-based inhibition of pulmonary inflammatory injury. To test this hypothesis, we first isolated the primary MenSCs according to a standard protocol, as shown in Figure S1A, following characterization by morphology and flow cytometry analysis (Figures S1B and S1C). Subsequently, the EVs released by MenSCs were collected using a stepwise ultracentrifugation procedure, as shown in Figure S2A. We then verified the specificity of EVs in light of the guidelines from the International Society for Extracellular Vesicles (ISEV).[34] Transmission electron microscopy (TEM) combined with nanoparticle flow cytometry (NanoFCM) analysis showed vesicles 50–150 nm in diameter with the classical saucer shape for these MenSC-isolated EVs (Figures S2B and S2C). Moreover, the characteristics of MenSC-EVs were further confirmed by western blot analysis (Figure S2D). To define the regulatory role of MenSCs and MenSC-EVs in pulmonary inflammatory injury, we intratracheally instilled MenSCs or MenSC-EVs into mouse lungs challenged with lipopolysaccharide (LPS) and assessed the effect of MenSCs and their released EVs on LPS-induced ALI. Notably, hematoxylin and eosin (H&E) and anti-CD68 immunohistochemistry (IHC) staining showed striking histological improvements of LPS-triggered pulmonary inflammatory injury after MenSCs or MenSC-EVs administration, as shown by alleviated alveolar congestion and neutrophil influx, thickened alveolar septa, and edema, as well as decreased alveolar macrophage infiltration (Figures 1A and 1B).

Moreover, we further measured the expression of inflammatory factors in the lungs of mice and found that the expression of inflammatory factors, including interleukin 1 beta (IL-1β), IL-6, tumor necrosis factor alpha (TNF-α), monocyte chemoattractant protein 1 (MCP-1), interferon gamma (IFN-γ), matrix metalloproteinase 9 (MMP-9), and granulocyte-macrophage colony stimulating factor (GM-CSF), were notably attenuated (Figure 1C). To further confirm the therapeutic role of MenSCs and MenSC-EVs in ALI, we extracted bronchoalveolar lavage fluid (BALF) from LPS-treated mice with or without MenSCs/MenSC-EVs administration and found that, compared with either vehicle control PBS or negative control normal

MenSC-EVs on the influx of inflammatory cells. The mice were sacrificed on day 4 after LPS stimulation (4 mg/kg). (G and H) The effect of MenSCs or MenSC-EVs on production of the proinflammatory cytokines IL-1β (G) and IL-6 (H) in BALF from mice treated with MenSCs, MenSC-EVs, or NHLF-EVs. The mice were sacrificed on day 4 after LPS stimulation (4 mg/kg). n = 5 per group (C–H); data are presented as mean ± SD. *$p < 0.05$, **$p < 0.01$, ***$p < 0.001$, and ****$p < 0.0001$ versus the injury group; #$p < 0.05$, ##$p < 0.01$, ###$p < 0.001$, and ####$p < 0.0001$ versus the NHLF-EVs group. All p values in this figure were obtained by one-way ANOVA. NHLF, normal human lung fibroblasts; BALF, bronchoalveolar lavage fluid; WBC, white blood cell; MPO, myeloperoxidase; BCA, bicinchoninic acid.

human lung fibroblast (NHLF)-EVs treatment, MenSCs and MenSC-EVs administration markedly reduced the alveolar protein permeability (Figure 1D). Consistent with this, this inhibitory role of MenSCs and MenSC-EVs in acute lung inflammation was further validated by the marked decline of white blood cell (WBC) counts and the activity of myeloperoxidase (MPO; a surrogate for neutrophil infiltration) in BALF from MenSC/MenSC-EV-treated mice relative to either PBS- or NHLF-EV-treated mice (Figures 1E and 1F). Similarly, secretion of proinflammatory cytokines, including IL-1β and IL-6, was also greatly impeded after MenSCs/MenSC-EVs administration, as measured by ELISA (Figures 1G and 1H).

Additionally, we performed high-throughput mRNA sequencing analysis to observe the MenSC/MenSC-EV-triggered changes in RNA expression profiles in the lungs of mice at the genomic level (Figure 2A). Consistent with the above finding, multiple biological processes associated with inflammatory injury response were functionally involved in the MenSC/MenSC-EV-mediated improvement of pulmonary inflammatory injury (Figure 2B). In line with this, the expression of the vast majority of regulators, particularly inflammatory factors, in the lungs of mice was significantly decreased upon MenSCs or MenSC-EVs treatment (Figure 2C). Overall, these findings strongly support that MenSC-released EVs have a similar inhibitory effect on acute lung inflammation and injury as MenSCs.

miR-671-5p is required for MenSC-EV-based improvement of ALI

Many studies have shown that EVs carry miRNAs as critical regulators responsible for EV-mediated remote communications between effector cells during the progression of acute lung inflammation and injury.[35] Therefore, we speculated that suppression of ALI by MenSC-EVs might depend on specific miRNAs carried by EVs. To prove this notion, we established miRNA profiles of MenSC-EVs using a small RNA microarray approach. Intriguingly, some miRNAs were identified, among which we further analyzed the top 25 miRNAs that were most abundantly expressed in MenSC-EVs (Figure S3A). Strikingly, miR-671-5p and miR-32-3p showed high sequence conservation among different species (Figure S3B). More importantly, quantitative PCR analysis exhibited a significant increase in expression of miR-671-5p (Figure 3A) but not miR-32-3p (Figure S3C) in the presence of LPS induction. This inflammatory injury-responsive change in miR-671-5p expression indicates a potential role in regulating acute lung inflammation and injury. More interestingly, the significant increase in expression of endogenous miR-671-5p in response to inflammatory injury suggests a possible compensatory mechanism to limit the progression of ALI.[36] Hence, we asked whether the miR-671-5p carried by MenSC-EVs could be transferred into lung epithelial cells through an EV-dependent pathway, thereby preventing the progression of pulmonary inflammatory injury.

To verify this hypothesis, the collected MenSC-EVs labeled by the fluorescent dye 3,3′-dioctadecyloxacarbocyanine perchlorate (DiO) were incubated with BEAS-2B cells to examine whether the EVs could be uptaken by pulmonary epithelial cells. As shown in Figure 3B, a large amount of MenSC-EVs was observed after incubation 12 h later. To further verify whether miR-671-5p could be delivered to the effector cells by these transmitted MenSC-EVs, we transfected the exogenously synthesized miR-671-5p mimic into MenSCs for subsequent *in vitro* incubation with BEAS-2B cells using a Transwell system. Notably, miR-671-5p-overexpressing MenSCs (Figure S3D), but not the scrambled control, showed efficient miR-671-5p transmission to BEAS-2B cells (Figure 3C). However, these transmitted miR-671-5p were abolished when the MenSCs were exposed to GW4869 (Figure 3C), a specific inhibitor for EVs, suggesting an EV-dependent manner for miR-671-5p transmission between MenSCs and BEAS-2B cells. Our results indicate that the MenSC-released miR-671-5p could be transferred into lung epithelial cells in an EV-dependent pathway for remote intercellular communication.

To verify whether MenSC-EV-transmitted miR-671-5p could help limit the progression of ALI, we first produced a lentivirus expressing a sponge competitively inhibit miR-671-5p and then transduced into MenSCs to deplete the endogenous miR-671-5p stably,[37] then collected the miR-671-5p-deficient MenSC-EVs, as well as empty vector-treated control MenSC-EVs, for subsequent intratracheal instillation into lungs of mice injured by LPS. Interestingly, miR-671-5p-deficient MenSC-EVs, rather than the control MenSC-EVs, showed failure to improve LPS-induced acute lung inflammation, as demonstrated by histological analysis (Figures 3D and 3E) and molecular assay (Figure 3F). To confirm abolishment of the beneficial effect from MenSC-EVs because of miR-671-5p deficiency, we extracted BALF from mice treated with miR-671-5p-deficient MenSC-EVs or control MenSC-EVs and measured the effects of these MenSC-EVs on pulmonary endothelial permeability and inflammation. Consistently, mice administered miR-671-5p-deficient MenSC-EVs presented higher total protein concentration, WBC counts, MPO activity, and proinflammatory cytokines compared with the control MenSC-EVs treatment (Figures 3G–3K). Altogether, these collective findings suggest a requirement of miR-671-5p for MenSC-EV-based improvement of acute lung inflammation and injury.

miR-671-5p negatively regulates acute lung inflammation and injury

The requirement of miR-671-5p in MenSC-EV-mediated improvement of pulmonary inflammatory injury prompted us to investigate the intrinsic capacity of miR-671-5p to regulate acute lung inflammation and injury. Using intratracheal instillation, we constructed an adeno-associated virus (AAV) vector carrying a sponge to deplete the endogenous miR-671-5p *in vivo*. The histological analysis indicated that miR-671-5p disruption significantly enhanced neutrophil infiltration, septal thickening, alveolar edema, and macrophage inflammatory infiltration (Figures 4A and 4B). In line with it, the levels of inflammatory factors in miR-671-5p-depleted lungs of mice were much higher than that in the empty vector-treated lungs of control mice (Figure 4C), which was consistent with the *in vitro* observations that miR-671-5p destruction crucially augmented the production of

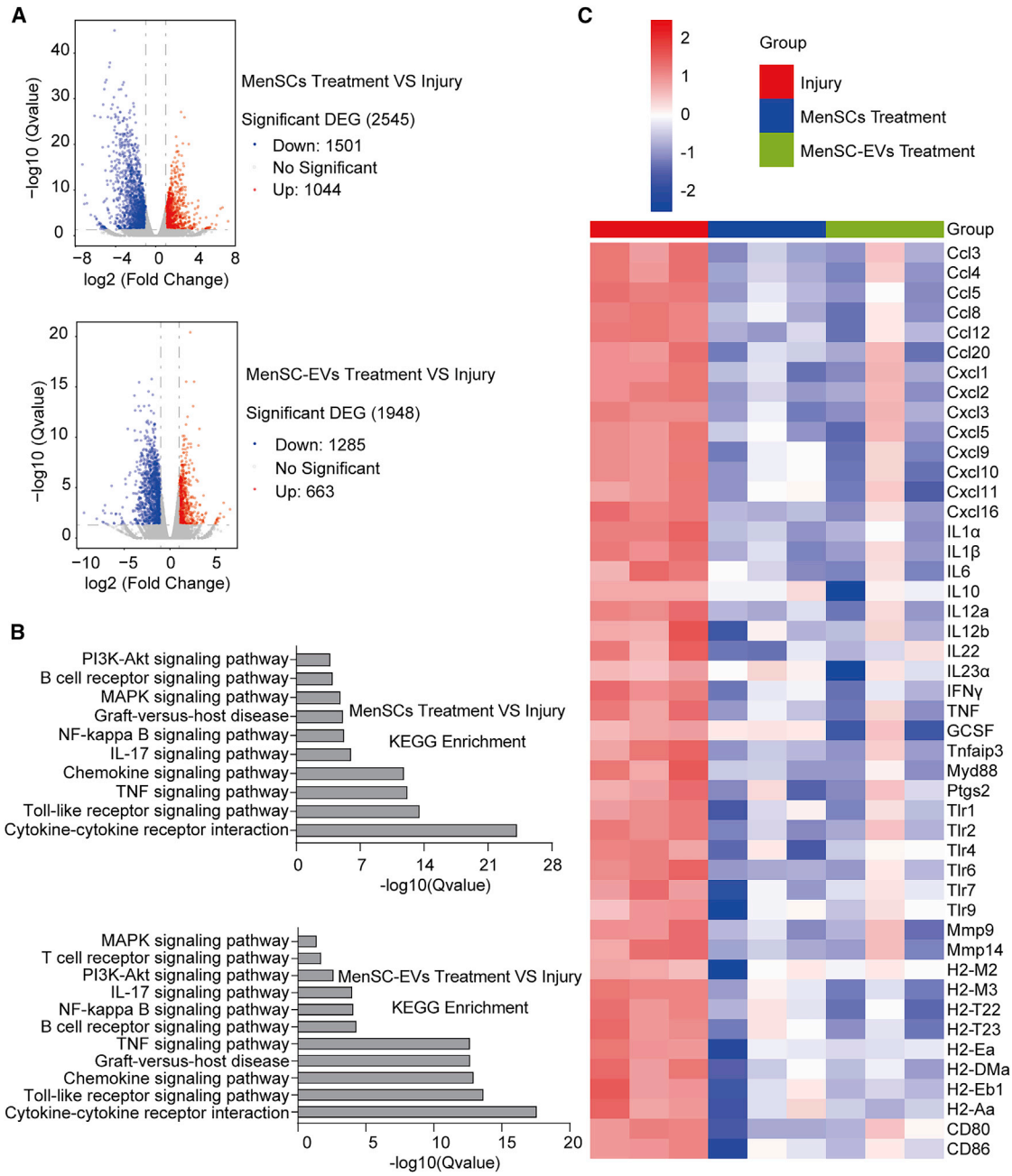

Figure 2. Comprehensive analysis of genes and pathways involved in MenSCs and MenSC-EVs treatment based on mRNA high-throughput sequencing

(A) Volcano plot of RNA-seq transcriptome data displaying the pattern of the gene expression profile in the lungs of mice with or without MenSCs or MenSC-EVs treatment. The mice were sacrificed on day 4 post LPS stimulation (4 mg/kg). Red and blue dots indicate significantly up- or down-regulated genes, respectively. $p < 0.05$, $|\log_2 FC| > 1$. (B) Kyoto Encyclopedia of Genes and Genomes (KEGG) enrichment analysis showing the inflammatory pathways involved in MenSC-based improvement of ALI. Total RNAs isolated from the lungs of mice with or without MenSCs or MenSC-EVs treatment in the presence of LPS stimulation (4 mg/kg) were subjected to RNA-seq analysis. (C) Representative heatmap of key factors involved in regulation of the inflammatory response based on the above mRNA-seq data. Red, relatively up-regulated expression; blue, relatively down-regulated expression. Each column represents one individual sample, and each row represents one single gene. n = 3 per group. DEG, differentially expressed gene. FC: fold change.

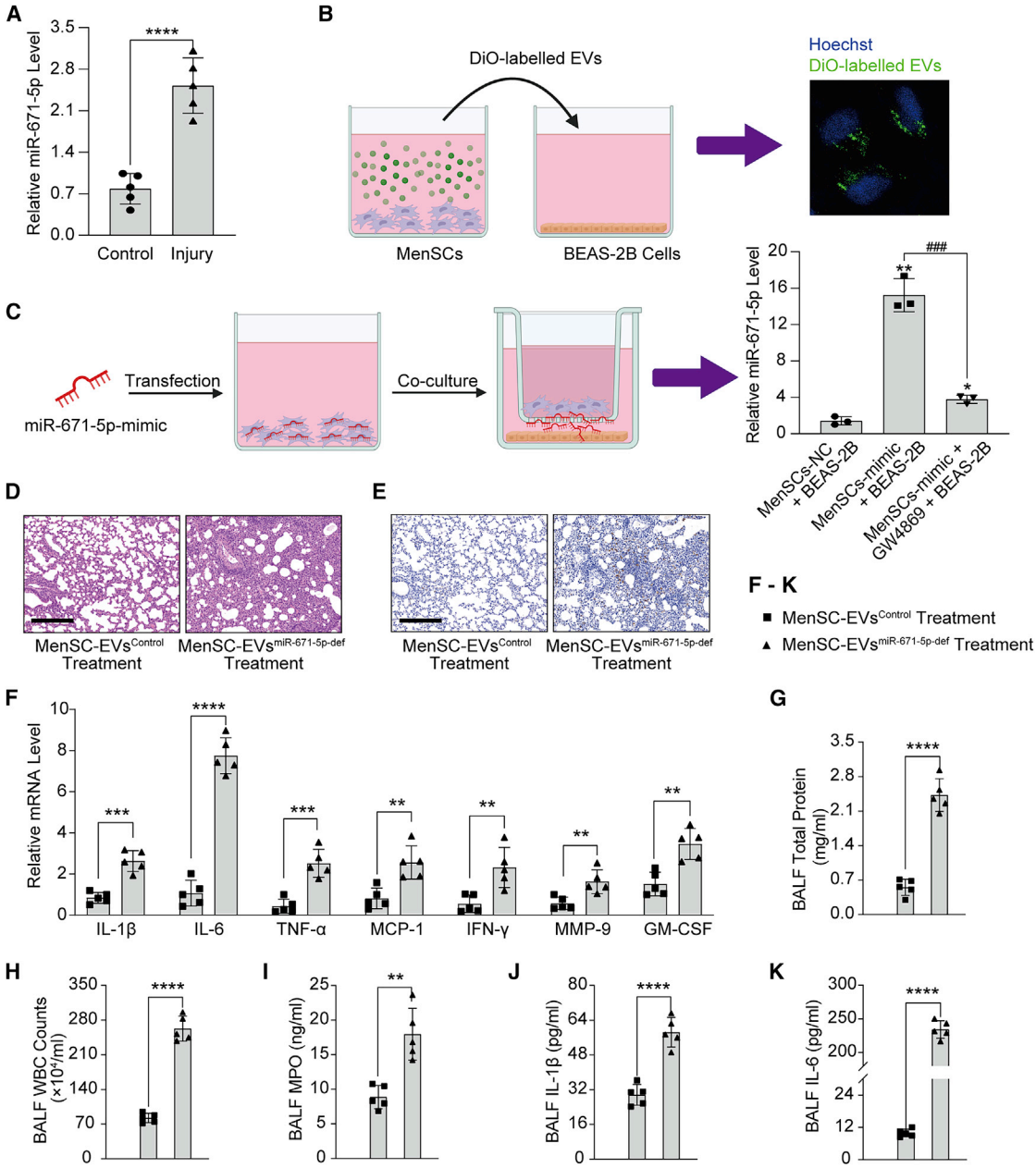

Figure 3. The improvement of ALI by MenSC-EVs depends on miR-671-5p transmitted by an EV-dependent pathway

(A) qRT-PCR analysis showing a robust elevation in miR-671-5p expression in the lungs of mice subjected to LPS stimulation (4 mg/kg). (B) Uptake assay showing the transfer of DiO-labeled MenSC-EVs into BEAS-2B cells. The MenSC-EVs were pre-labeled with DiO for 15 min before incubation with BEAS-2B cells. (C) miR-671-5p is transferred from MenSC-EVs to pulmonary epithelial cells by an EV-dependent pathway. MenSCs overexpressing the miR-671-5p mimic were pre-treated with GW4869 (10 μM) or a vehicle control for 24 h and then incubated with BEAS-2B cells in a Transwell plate. (D and E) Depletion of miR-671-5p in MenSCs reduced the therapeutic effect of MenSC-EVs on ALI, as detected by H&E staining (D) and CD68 IHC staining (E) of lung sections from mice administered EVs isolated from MenSCs stably expressing a sponge depleting miR-671-5p or an empty vector control. The mice were sacrificed on day 4 after LPS stimulation (4 mg/kg). Scale bar, 200 μm. (F) The relative mRNA levels of proinflammatory cytokines in lungs of mice administrated EVs isolated from MenSCs stably expressing a sponge depleting miR-671-5p or an empty vector control were measured by qRT-PCR. (G–K) Total protein concentration (G), WBC counts (H), MPO activity (I), and production of the proinflammatory factors IL-1β (J) and IL-6 (K) in BALF from mice administered EVs isolated from MenSCs stably expressing a sponge depleting miR-671-5p or an empty vector control were measured to determine the effect of miR-671-5p deficiency on EV-mediated amelioration of ALI. n = 3 per group (C); data are presented as mean ± SD. *p < 0.05, **p < 0.01, ***p < 0.001, and ****p < 0.0001; p value was calculated by one-way ANOVA compared with the MenSCs-NC + BEAS-2B group. #p < 0.05, ##p < 0.01, ###p < 0.001, and ####p < 0.0001, p value was calculated by Student's t test. n = 5 per group (A and F–K); data are presented as mean ± SD. *p < 0.05, **p < 0.01, ***p < 0.001, and ****p < 0.0001; all p values in this figure were obtained by Student's t test. NC, negative control; mimic, miR-671-5p-mimic; def, deficient.

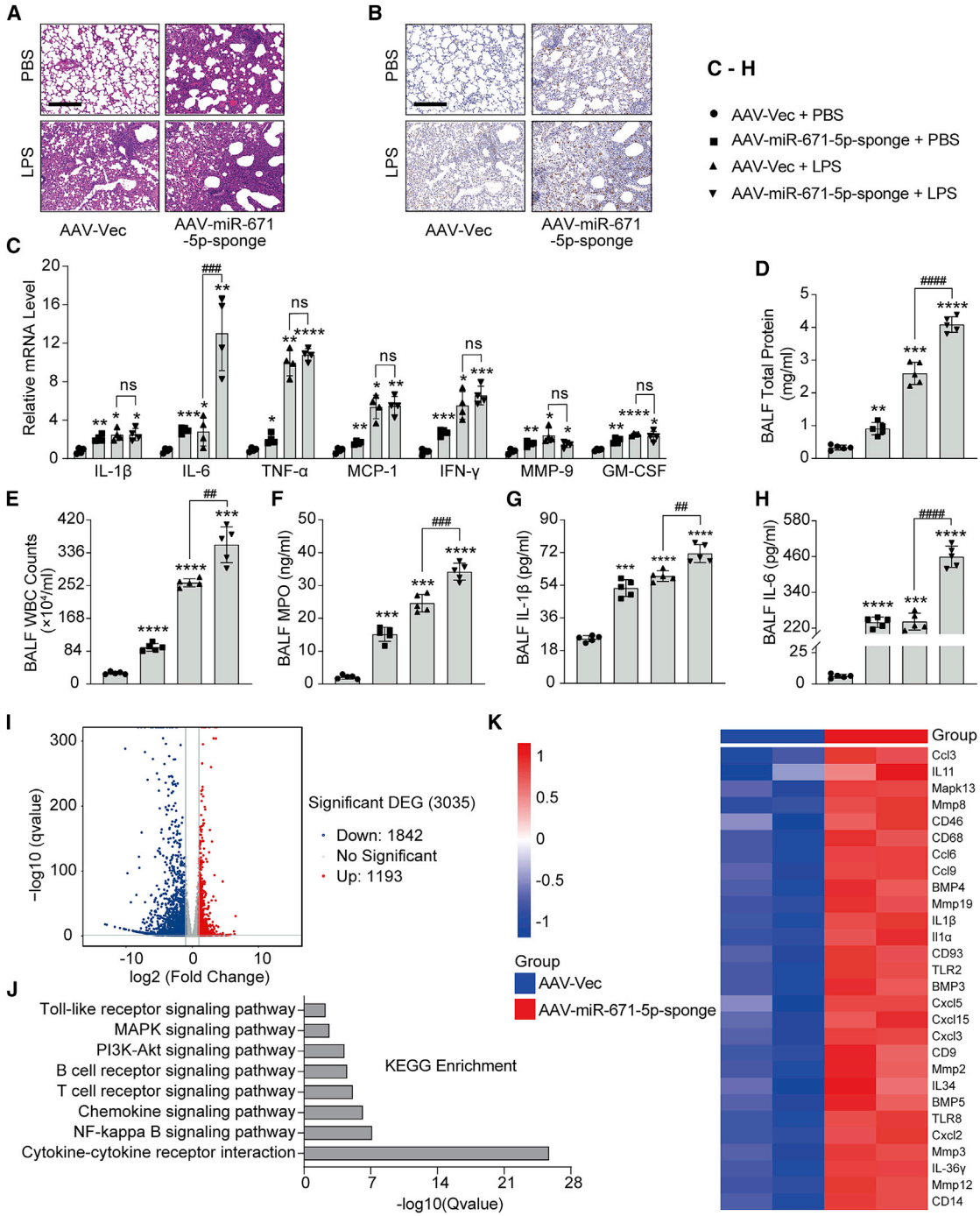

Figure 4. miR-671-5p negatively regulates acute lung inflammation and injury

(A) The effect of miR-671-5p depletion on ALI, as assayed by H&E staining of lung sections from mice with or without AAV-mediated miR-671-5p knockdown. The mice were treated with LPS (4 mg/kg) or a vehicle control after 3 weeks of AAV infection. Scale bar, 200 μm. (B) The effect of AAV-mediated miR-671-5p depletion on the accumulation of pulmonary macrophages, as detected by CD68 IHC staining of lung sections from mice with or without AAV-mediated miR-671-5p knockdown. Scale bar, 200 μm. (C) The effect of AAV-mediated miR-671-5p depletion on the expression of proinflammatory factors in the lungs of mice treated with or without LPS, as determined by qRT-PCR assay. (D–H) Total protein concentration (D), WBC counts (E), MPO activity (F), and production of the proinflammatory factors IL-1β (G) and IL-6 (H) in BALF from mice with or without miR-671-5p depletion were detected to examine the influence of miR-671-5p on pulmonary inflammatory injury. The mice were treated with LPS (4 mg/kg) or a vehicle control after 3 weeks of AAV infection. (I–K) Lung tissues isolated from mice receiving the AAV-expressing miR-671-5p sponge or an empty vector control were

(legend continued on next page)

these proinflammatory factors in primary AT2 and BEAS-2B cells with or without LPS stimulation (Figures S4A and S4B). Moreover, we also assessed BALF from lungs with or without miR-671-5p destruction and found that, similar to the histological observations, the total protein concentration, WBC counts, MPO activity, as well as production of inflammatory factors in BALF from mice with miR-671-5p depletion were markedly induced in the presence or absence of LPS induction (Figures 4D–4H). These results strongly support the crucial inhibitory role of miR-671-5p in acute lung inflammation and injury.

To further validate the significant inhibition of pulmonary inflammatory injury conferred by miR-671-5p at the molecular level, we performed high-throughput mRNA sequencing analysis of lungs of mice with or without miR-671-5p depletion (Figure 4I). Unsurprisingly, most inflammatory cytokines and chemokines, including CCL3, CCL6, CCL9, IL-1β, and IL-1α, were markedly augmented under miR-671-5p inhibition (Figure 4K). Furthermore, enrichment analysis of Kyoto Encyclopedia of Genes and Genomes (KEGG) pathways demonstrated that miR-671-5p was tightly linked to classic inflammatory pathways such as NF-κB, mitogen-activated protein kinase (MAPK), TLR, and phosphatidylinositol 3-kinase (PI3K)-Akt signaling pathways (Figure 4J). These molecular studies were consistent with the *in vivo* observations described above, highlighting the critical inhibitory function of miR-671-5p during the progression of acute lung inflammation and injury.

miR-671-5p alleviates pulmonary inflammatory injury through posttranscriptional regulation of AAK1

To explore the precise molecular mechanism by which miR-671-5p negatively regulates acute lung inflammation and injury, we employed predictor tools to identify the downstream targets of miR-671-5p. Interestingly, "TargetScan" and "miRDB," two widely used predictors for miRNAs, identified AAK1 as a potential candidate. Of note, AAK1 has been reported previously to positively regulate the inflammatory response, indicating that AAK1 is likely to be the key downstream target by which miR-671-5p modulates lung inflammation and injury. Further analysis by the predictors helped us define two strong seed regions within the 3′ UTR of AAK1 mRNA (Figure S5B). Moreover, sequence alignment showed high conservation of AAK1 among different species (Figure S5C). A significant negative correlation between AAK1 and miR-671-5p RNA expression upon inflammatory injury triggered by LPS was also observed by quantitative PCR analysis (Figures 3A and 5A). More importantly, AAV-mediated miR-671-5p depletion greatly enhanced AAK1 mRNA expression *in vivo* (Figure 5B), and lentivirus-mediated miR-671-5p overexpression strongly inhibited AAK1 mRNA levels in BEAS-2B and AT2 cells (Figure S4C). These findings raised a possibility that AAK1 might be the downstream effector protein in miR-671-5p-mediated suppression of pulmonary inflammatory injury. To prove this notion, we first generated an SV40 promoter-driven luciferase reporter carrying a synthesized AAK1 3′ UTR DNA fragment with or without the seed site mutation (i.e., AAK1-3′ UTR-wild type [WT] and AAK1-3′ UTR-mutant [Mut]) (Figures S5A and S5B), and then evaluated luciferase activity in the presence or absence of miR-671-5p overexpression to ascertain whether AAK1 is a direct target of miR-671-5p. As predicted, miR-671-5p overexpression critically blocked the activity of the luciferase reporter carrying the WT AAK1 seed region, while the mutated AAK1 seed region-containing reporter showed significant resistance to the inhibitory effect of miR-671-5p (Figures 5C and S5D). Additionally, the sponge for miR-671-5p remarkably impeded miR-671-5p overexpression-triggered downregulation of AAK1 luciferase activity (Figures 5C and S5D). These collective findings suggest that AAK1 is a direct downstream target of miR-671-5p.

We next sought to characterize the functional involvement of AAK1 in acute lung inflammation and injury. Histological assays demonstrated that AAV-based AAK1 depletion strongly impeded LPS-induced neutrophil infiltration, septal thickening, alveolar edema, and macrophage inflammatory infiltration, as detected by H&E staining and anti-CD68 IHC staining analysis (Figures 5E and 5F). In line with this, AAK1 disruption dramatically restrained the expression levels of the proinflammatory factors because of LPS induction in the lungs of mice *in vivo* (Figures 5D and 5G) as well as in primary AT2 and BEAS-2B cells *in vitro* (Figures S5E and S5F). To further ascertain the inhibitory role of AAK1 in acute pulmonary inflammatory injury, we extracted BALF from mice infected with AAV-expressing AAK1 short hairpin RNA (shRNA) or scrambled control and analyzed the alveolar permeability and inflammation. As expected, BALF from mice infected with AAK1 shRNA showed lower levels of total protein concentration, WBC counts, MPO activity, and proinflammatory factor secretion compared with the control group after LPS stimulation (Figures 5H–5L). These observations demonstrate that miR-671-5p negatively regulates pulmonary inflammatory injury, at least partially, through posttranscriptional regulation of AAK1.

AAK1 disruption rescues the reduced ameliorative effect of MenSC-EVs on ALI caused by miR-671-5p deficiency

Considering the positive regulation of lung inflammation and injury by AAK1, a direct target of miR-671-5p, as evidenced above, we asked whether AAK1 is required for miR-671-5p-mediated improvement of pulmonary inflammatory injury. To test this

subjected to high-throughput mRNA sequencing analysis to detect the effect of miR-671-5p depletion on downstream gene expression profiles and signaling pathways. A representative graph shows the up- or down-regulated genes (I), a KEGG enrichment analysis shows the downstream pathways regulated by miR-671-5p (J), and a representative heatmap shows the expression changes of the indicated factors (K). n = 4 per group (C), n = 5 per group (D–H); data are presented as mean ± SD. *p < 0.05, **p < 0.01, ***p < 0.001, and ****p < 0.0001 compared with the AAV-vector (Vec) + PBS group; ns, not significant, #p < 0.05, ##p < 0.01, ###p < 0.001, and ####p < 0.0001 for comparisons between the indicated groups. A Student's t test and one-way ANOVA were used to compare two groups and multiple groups. n = 3 per group (I–K). AAV, adeno-associated virus.

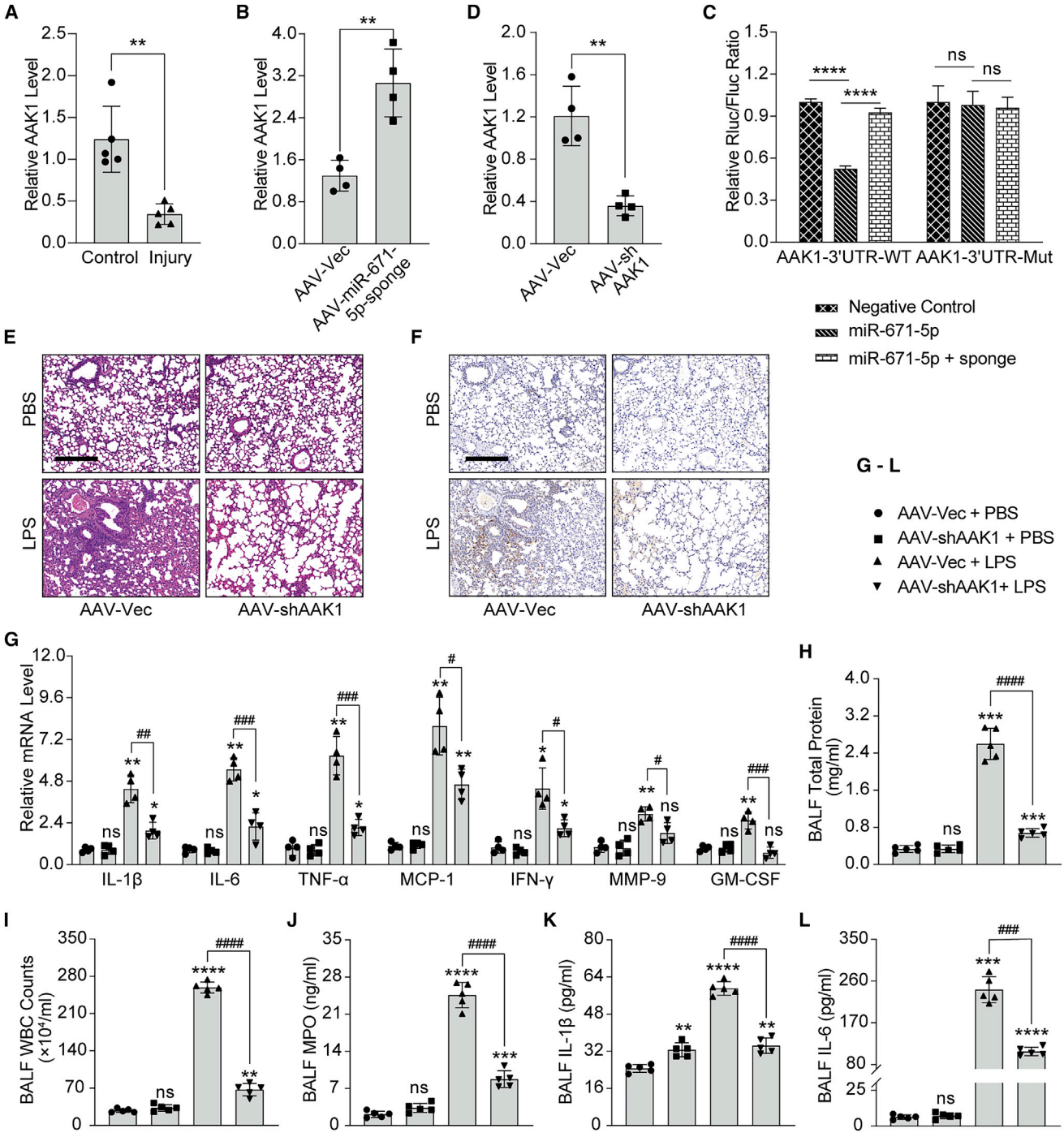

Figure 5. AAK1, a direct target of miR-671-5p, positively regulates lung inflammation and injury in LPS-induced ALI mice

(A) qRT-PCR analysis of lung tissues from mice treated with or without LPS (4 mg/kg), showing the markedly declined AAK1 RNA level in response to LPS induction. (B) qRT-PCR analysis showing the effect of AAV-mediated miR-671-5p depletion on AAK1 expression in lung tissues of mice subjected to 3 weeks of AAV infection. (C) Dual-luciferase reporter assay showing that AAK1 is a direct target of miR-671-5p. The seed region (nt 685–692) within the 3′ UTR of AAK1 or its Mut form was cloned into an SV40 promoter-driven luciferase reporter. (D) qRT-PCR analysis showing the AAV-mediated knockdown efficiency of AAK1 shRNA in lung tissues of mice receiving 3 weeks of AAV-shAAK1 infection. (E and F) AAV-mediated AAK1 disruption alleviates LPS-induced pulmonary inflammatory injury. Mice administered the AAV-expressing AAK1 shRNA or a mock control were subjected to histological analysis after LPS or PBS treatment. Shown are H&E staining analysis (E) and CD68 IHC histological analysis (F). Scale bar, 200 μm. (G) The effect of AAV-mediated AAK1 shRNA knockdown on expression of inflammatory mediators in lungs of mice injured with LPS (4 mg/kg) or a vehicle PBS

(legend continued on next page)

hypothesis, AAV-expressing AAK1 shRNA was first instilled intratracheally into the lungs of mice, followed by additional control MenSC-EVs or miR-671-5p-deficient MenSC-EVs administration to prove whether AAK1 is a crucial downstream target for miR-671-5p-modulated alleviation of ALI (Figure 6A). Strikingly, AAK1 disruption led to almost total abrogation of miR-671-5p deficiency-induced inflammatory injury, as shown by H&E and anti-CD68 IHC staining (Figures 6B and 6C). Consistent with this, AAK1 depletion profoundly attenuated the increased expression of inflammatory factors in lung tissues induced by miR-671-5p-deficient MenSC-EVs treatment (Figure 6D). The requirement of AAK1 in miR-671-5p mediated pulmonary inflammatory injury was further confirmed by the BALF results, as shown by the significantly alleviated total protein concentration, WBC counts, MPO activity, and proinflammatory factor production in BALF from mice with AAK1 and miR-671-5p double depletion compared with that from mice with only miR-671-5p depletion (Figures 6E–6I). Altogether, these collective findings led us to conclude that AAK1 is indispensable in regulating acute lung inflammation and injury by miR-671-5p.

AAK1 regulates the activity of NF-κB signaling

The significance of the miR-671-5p/AAK1 axis in pulmonary inflammatory injury prompted us to investigate the underlying molecular mechanism by which AAK1 triggers activation of inflammatory injury. According to the mRNA sequencing data in Figure 4J, the NF-κB signaling pathway regulates pulmonary inflammatory injury by miR-671-5p. Therefore, we speculate that, as a downstream target of miR-671-5p, AAK1 might be a crucial upstream regulator responsible for activating NF-κB signaling. To examine this, we first performed immunoblot analysis to determine the effects of AAK1 on the stability of p65 or IκBα, a critical inhibitory protein of NF-κB. Notably, AAK1 knockdown led to a marked decrease in IκBα degradation, whereas the p65 level did not appear to be influenced (Figure 7A). Next, we performed p65 affinity purification from cells expressing the exogenous FLAG-tagged p65 and then quantified the phosphorylation level of p65 with or without AAK1 knockdown, using a phospho-specific antibody targeting p65 S536 phosphorylation that is well known to activate NF-κB signaling. We found that knocking down AAK1 strongly attenuated the S536 phosphorylation of p65 (Figure 7B). Consistent with this, acetylation of p65 at the K310 site, widely accepted as another modification to trigger NF-κB activation, showed a marked decrease after AAK1 depletion (Figure 7B). To further confirm the inhibitory effect on NF-κB signaling activation conferred by AAK1 depletion, we performed a ubiquitination assay and found that AAK1 disruption significantly prevented ubiquitin-mediated IκBα degradation (Figure 7C). In addition, we also constructed an AAK1-overexpressing vector to verify the positive regulation of NF-κB signaling by AAK1. Immunoblot analysis showed an obvious increase in ubiquitin-mediated IκBα degradation after AAK1 overexpression (Figures 7D and 7F), which is consistent with the increased p65 S536 phosphorylation and K310 acetylation caused by the highly expressed AAK1 level (Figure 7E). In summary, these observations suggest that AAK1 positively regulates NF-κB signaling activity.

miR-671-5p has a significant negative correlation with AAK1 in pulmonary inflammatory disease

The functional importance of the miR-671-5p/AAK1 axis in pulmonary inflammatory injury promoted us to study its clinical relevance. For this purpose, we collected injured pulmonary samples paired with corresponding adjacent normal samples from patients with organizing pneumonia and then determined their expression changes after an inflammatory injury. Notably, a FISH assay indicated that the expression of miR-671-5p was greatly decreased in the lesion areas of lungs from patients with organizing pneumonia compared with the corresponding normal areas (Figure 8A). Additionally, similar results were verified by quantitative PCR analysis (Figure 8B). In contrast, as determined by quantitative PCR analysis, the AAK1 expression levels were correspondingly increased in the lesion areas relative to the normal control areas (Figure 8C). This significant negative correlation between miR-671-5p and AAK1 in pulmonary inflammatory disease is consistent with the observations obtained from *in vivo* mouse models showing that LPS induction strongly induced miR-671-5p levels in the lungs of mice but dampened AAK1 expression. Clinical studies and mouse pulmonary inflammatory models demonstrate that miR-671-5p has a significant negative correlation with AAK1 in pulmonary inflammatory disorders.

DISCUSSION

Uncontrolled inflammation is the main cause of high mortality in individuals with ARDS and COVID-19, and molecularly targeted therapies that minimize pulmonary inflammation and injury could improve clinical outcomes. Studies from other groups in animal models and human patients of acute lung inflammation and injury have proven that administration of MSC-EVs duplicated the beneficial protection of their parent MSCs.[32,38,39] However, a complete understanding of the mechanisms of the therapeutic potential of MSC-EVs in acute lung inflammation and injury remains an important gap in our knowledge. The data collected in this study may offer new convincing theoretical evidence for MenSC-EVs as a promising strategy to ameliorate inflammation and injury in acute lung inflammatory disorders, especially the emerging human infectious disease COVID-19, which is similar to the LPS-induced ALI model with consistent pathological characteristics.[40,41] Our

control. The mice were injured with LPS 3 weeks after AAV infection. (H–L) Total protein concentration (H), WBC counts (I), MPO activity (J), as well as production of the proinflammatory factors IL-1β (K) and IL-6 (L) in BALF from mice with or without AAK1 disruption were detected to examine the influence of AAK1 disruption on pulmonary inflammatory injury. The lungs of mice were treated with LPS (4 mg/kg) or a vehicle PBS control after 3 weeks of AAV infection. n = 5 per group (A and H–L), n = 4 per group (B, D, and G), and n = 3 (C); data are presented as mean ± SD. *$p < 0.05$, **$p < 0.01$, ***$p < 0.001$, and ****$p < 0.0001$ compared with the AAV-Vec + PBS group; #$p < 0.05$, ##$p < 0.01$, ###$p < 0.001$, and ####$p < 0.0001$ for comparisons between the indicated groups. A Student's t test and one-way ANOVA were used to compare two groups and multiple groups. WT, wild type; Mut, mutant; sponge, miR-671-5p-sponge.

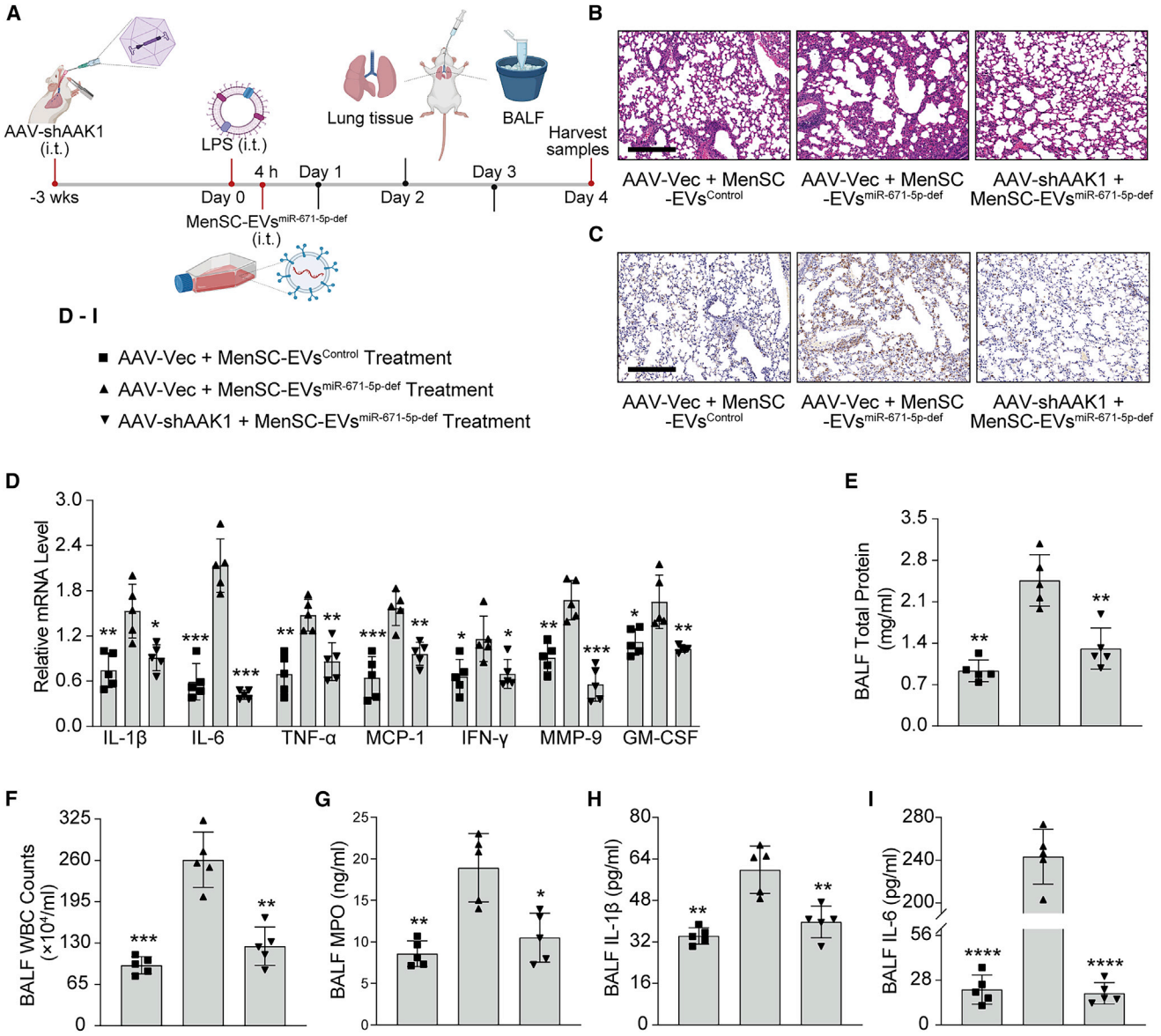

Figure 6. Disruption of AAK1 reverses the reduced protective effect of MenSC-EVs on ALI caused by miR-671-5p deficiency

(A) Schematic showing the detailed procedure for the combined AAV-shAAK1 and MenSC-EVs treatment mouse model study; created with BioRender. (B and C) Representative H&E (B) and CD68 IHC (C) staining of lung sections from mice administered the combined EVs isolated from MenSCs stably expressing a sponge depleting miR-671-5p or an empty Vec control and AAK1 shRNA or a mock control. The mice were sacrificed on day 4 after LPS stimulation (4 mg/kg). Scale bar, 200 μm. (D) qRT-PCR analysis of inflammatory mediator expression levels in lungs of mice treated with the combined EVs isolated from MenSCs stably expressing a sponge depleting miR-671-5p or an empty Vec control and AAK1 shRNA or a mock control. The mice were sacrificed on day 4 after LPS stimulation (4 mg/kg). (E–I) Total protein concentration (E), WBC counts (F), MPO activity (G), and production of the proinflammatory factors IL-1β (H) and IL-6 (I) in BALF from mice administered the combined EVs isolated from MenSCs stably expressing a sponge depleting miR-671-5p or an empty Vec control and AAK1 shRNA or a mock control. The mice were sacrificed on day 4 after LPS stimulation (4 mg/kg). n = 5 per group; data are presented as mean ± SD. *$p < 0.05$, **$p < 0.01$, ***$p < 0.001$, and ****$p < 0.0001$ compared with the AAV-Vec + MenSC-EVs$^{miR-671-5p-def}$ treatment group. One-way ANOVA was used to obtain all p values in this figure.

study provides first-hand evidence of the potential molecular mechanism by which MenSC-EVs improve acute lung inflammation and injury through transmitting miR-671-5p in an EV-dependent manner.

In the present study, we strongly demonstrated that human MenSCs were a good source of EVs for ALI protection in cell-free therapy. Our findings, using the LPS-induced ALI mouse model, suggested that MenSC-EVs and their parent MenSCs had a similar

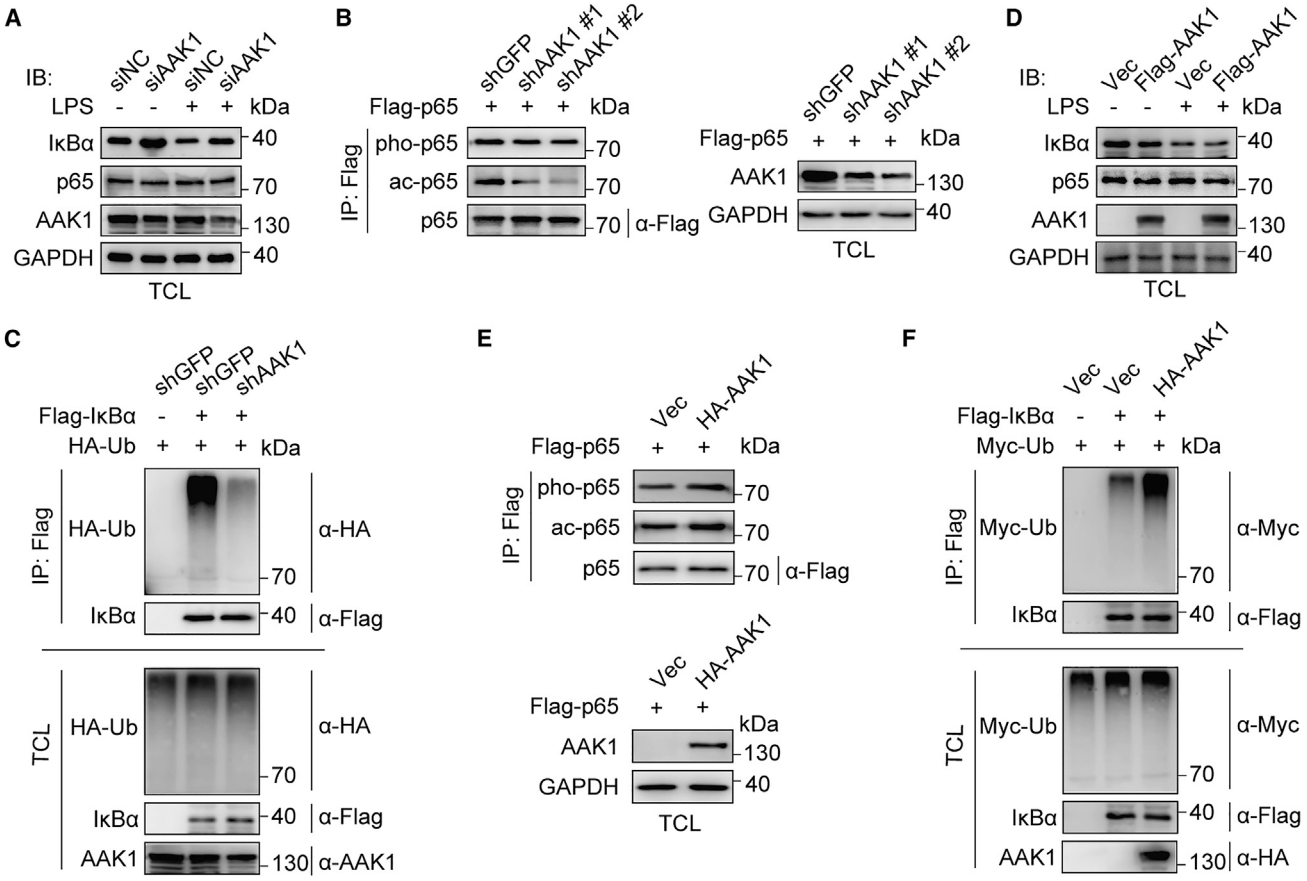

Figure 7. AAK1 activates the NF-κB signaling pathway by controlling IκBα stability

(A) Immunoblot analysis of IκBα and p65 expression in total lysates of BEAS-2B cells transfected with AAK1 siRNA or an NC in the presence or absence of LPS (100 ng/mL, 24 h). (B) Immunoblot analysis of p65 S536 phosphorylation (pho) and K310 acetylation (ac) levels in the immunoprecipitates from BEAS-2B cells transduced with a lentivirus expressing AAK1 shRNA or the shGFP control by anti-p65 immunoprecipitation. The knockdown efficiency of AAK1 in total lysates of BEAS-2B cells is shown on the right. (C) Immunoblot analysis of IκBα ubiquitination in total lysates of HEK293T cells expressing the indicated combinations of FLAG-tagged IκBα, HA-tagged ubiquitin, and AAK1 shRNA or the shGFP control. The cells were treated with MG-132 (20 μM, 4 h) before collection. (D) Immunoblot analysis of IκBα and p65 expression in total lysates of BEAS-2B cells transduced with a lentivirus expressing FLAG-tagged AAK1 or an empty Vec control in the presence or absence of LPS (100 ng/mL, 24 h). (E) Immunoblot analysis of p65 S536 phosphorylation and K310 acetylation levels in the immunoprecipitates from BEAS-2B cells transduced with a lentivirus overexpressing AAK1 or an empty Vec control by anti-p65 immunoprecipitation. AAK1 reintroduction in BEAS-2B cells was verified by immunoblot analysis of the total lysates (bottom panel). (F) Immunoblot analysis of IκBα ubiquitination in total lysates of HEK293T cells expressing the indicated combinations of FLAG-tagged IκBα, Myc-tagged ubiquitin, and HA-tagged AAK1 or empty Vec. The cells were treated with MG-132 (20 μM, 4 h) before collection.

therapeutic potency *in vivo*. Notably, compared with the LPS-injured model group, MenSC- and MenSC-EV-administered groups showed an obvious resistance to major histocompatibility complex (MHC) expression (Figure 2C), as reflected by the enriched Graft versus Host Disease (GVHD) pathway (Figure 2B). Hence, MenSC-based transplantation is a beneficial strategy for the treatment of pulmonary inflammatory disorders largely due to their low immunogenicity.

More studies have shown that EVs can participate in remote cellular functional regulation by transmitting specific miRNAs to recipient cells.[42–47] We established the miRNA profiles of MenSC-EVs for high-throughput microarray analysis. Combined with the compensatory increase in endogenous miR-671-5p in response to ALI, the abundantly expressed miR-671-5p, which is highly conserved among different species in MenSC-EVs, was identified as a central regulator for MenSC-EV-mediated improvement of acute lung inflammation and injury. More importantly, depletion of miR-671-5p in MenSCs substantially reduced the therapeutic effect of MenSC-EVs on acute lung inflammation and injury, consistent with functional studies showing that miR-671-5p disruption profoundly triggers activation of multiple inflammatory signaling pathways, as evidenced by mRNA sequencing analysis. Additionally, our *in vitro* investigations showed that miR-671-5p could be transmitted into epithelial cells in lung tissues, such as BEAS-2B cells, in an EV-dependent manner. Thus, MenSC-EV-mediated miR-671-5p delivery to lung tissue

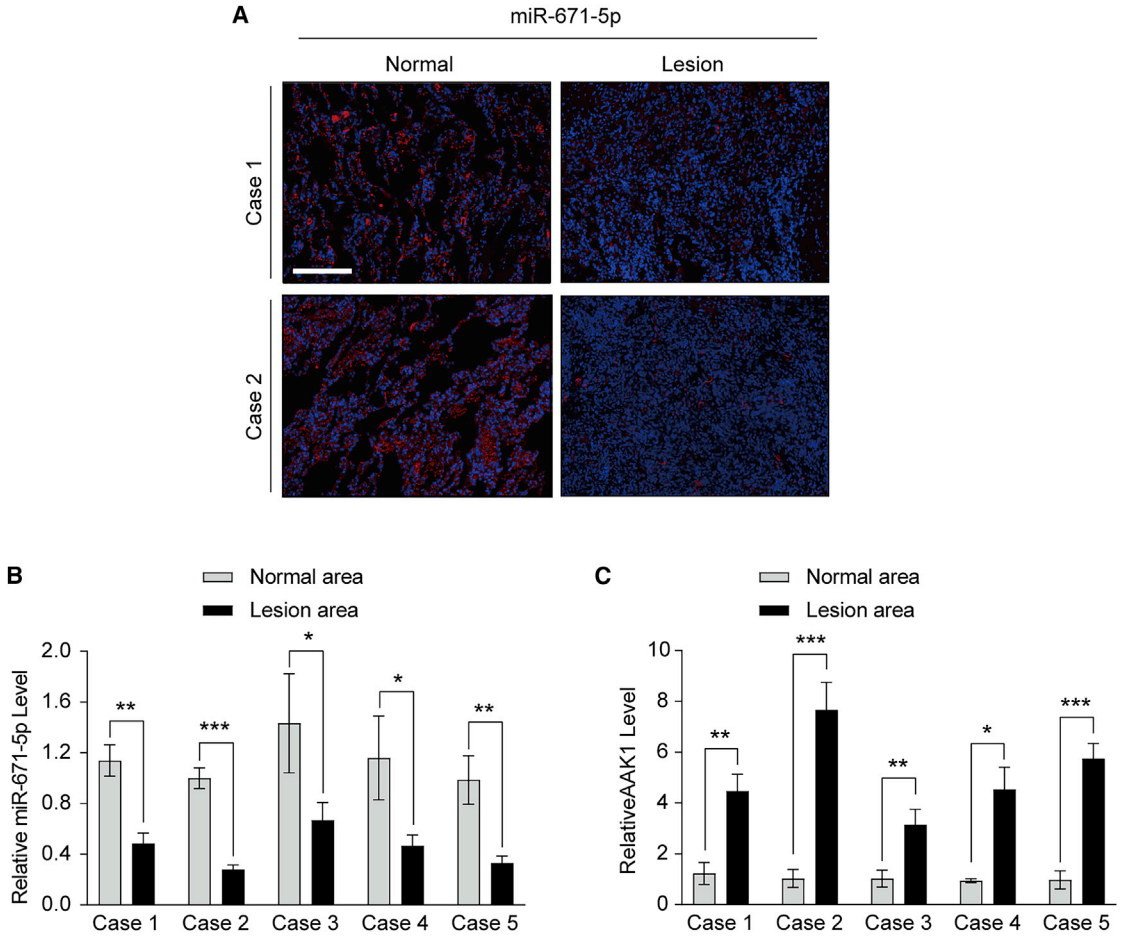

Figure 8. miR-671-5p has a significant negative correlation with AAK1 in pulmonary inflammatory disease

(A) Representative images of lung sections from lesion areas or corresponding adjacent normal areas of 2 different patients with organizing pneumonia, showing the expression levels of miR-671-5p, as determined by FISH assay. Scale bar, 200 μm. (B and C) qRT-PCR analysis of miR-671-5p (B) and AAK1 (C) expression in inflammatory lesion areas or corresponding adjacent normal areas of lung tissues from 5 different patients with organizing pneumonia. n = 3 (B and C), representing 3 pairs of samples from one individual patient; data are presented as mean ± SD. *$p < 0.05$, **$p < 0.01$, and ***$p < 0.001$ for comparisons between the indicated groups. All p values in this figure were obtained by Student's t test.

should be an effective strategy for mitigating LPS or other pathogen-induced pulmonary inflammation and injury.

Despite some evidence showing engagement of miR-671-5p in modulating pulmonary inflammatory injury,[48] the underlying molecular basis of how miR-671-5p impedes lung inflammation and injury has not been illustrated until now. The current study identifies the kinase AAK1 as a direct target of miR-671-5p. Of importance, AAK1 depletion rescues the reduced therapeutic effect of MenSC-EVs on pulmonary inflammatory injury caused by miR-671-5p deficiency, suggesting that AAK1 is likely to be a central downstream effector protein in miR-671-5p-mediated improvement of acute lung inflammation and injury. AAK1 was previously known as a crucial regulator responsible for CME of the virus, including SARS-CoV-2.[24–28,49,50] However, the intrinsic regulatory role of AAK1 in signal transduction remains poorly understood. Here we characterize AAK1 as a vital activator of NF-κB signaling. AAK1 destruction dramatically impaired ubiquitin-mediated IκBα degradation, blocking activation of NF-κB signaling. These observations suggest another regulatory role of AAK1 in viral or bacterial infection-induced pulmonary inflammatory disorders. Besides regulation of endocytosis to facilitate virus infection, as previously illustrated, AAK1 activates acute lung inflammation and injury, perhaps more importantly, through modulating its downstream inflammatory signaling, particularly NF-κB signaling. Additionally, a significant negative correlation between miR-671-5p and AAK1 was also observed in clinical organizing pneumonia, highlighting the critical regulatory function of the miR-671-5p/AAK1 axis in clinical pulmonary inflammatory diseases. More interestingly, the inflammatory injury in clinical samples of organizing pneumonia and lungs of mice injured by LPS shows opposite

changes in expression of miR-671-5p, which indicates a rapid compensatory mechanism to limit the progression of pulmonary inflammatory injury in response to LPS stimulation. In the LPS-induced mouse model, miR-671-5p was rapidly increased in response to this acute pulmonary inflammation. This regulatory pattern provides a compensatory manner to immediately acquire enough miR-671-5p to improve the pulmonary inflammatory injury. However, for clinical patients with organizing pneumonia, it might involve a long-term regulatory pattern for chronic inflammatory injury. During the development of organizing pneumonia, miR-671-5p becomes unstable and gradually loses its inhibitory function on pulmonary inflammation, consequently leading to dysregulation of this inflammatory disorder. We propose that this might be the major reason that led to the distinct regulatory patterns in response to acute or chronic pulmonary inflammatory injury. In summary, our study provides strong evidence showing the functional importance of the miR-671-5p/AAK1 axis in MSC-based improvement of pulmonary inflammatory injury, and targeting the miR-671-5p/AAK1 axis might be a good strategy for MSC-based therapy of pulmonary inflammatory disorders in the future.

MATERIALS AND METHODS

MenSCs culture and MenSC-EVs isolation

MenSCs were obtained from healthy young female individuals (aged 25–35) and provided by the Zhongyuan Stem Cell Research Institute of the Xinxiang High Tech Zone. The third to fifth passages of MenSCs were cultured for subsequent experiments. MenSCs were cultured in Dulbecco's modified Eagle's medium (DMEM; Gibco, USA) with 10% Fetal Bovine Serum (FBS, Gibco, USA) and 1% penicillin-streptomycin (Corning, USA) at 37°C in a humidified 5% CO_2 incubator. When MenSCs were cultured to 70%–80% confluency, they were ready for further use. MenSCs were identified with a human MSC analysis kit (562245, BD Biosciences, USA) by flow cytometry analysis. EVs were obtained from the supernatants of MenSCs or NHLF (CC-2512, Lonza, Switzerland) culture over 48 h in DMEM with 10% EV-depleted FBS or fibroblast basal medium (FBM; CC-3131, Lonza, Switzerland) with 2% EV-depleted FBS, which was also obtained by ultracentrifugation (100,000 × *g* for 18 h at 4°C), conforming to MISEV2018.[34] To isolate the EVs, cell-free conditioned medium was obtained by differential ultracentrifugation (XPN-100, Beckman Coulter, USA), which followed previously protocols,[51] as shown in Figure S2A. The isolated MenSC-EVs were characterized by TEM (HT-7700, Hitachi, Japan) and nanoparticle flow cytometry (N30E, NanoFCM, China), and surface markers of EVs, including CD9 (20597-1-AP, Proteintech, China), CD63 (25682-1-AP, Proteintech, China), CD81 (27855-1-AP, Proteintech, China), and Alix (2171S, Cell Signaling Technology, USA), were identified by western blot. The harvested MenSCs, MenSC-EVs, and NHLF-EVs were resuspended in PBS for subsequent animal study.

Intratracheal administration of MenSCs or MenSC-EVs for the LPS-induced ALI mouse model

This study was performed following approval from the Ethics Committee of Xinxiang Medical University. All animal experiments were implemented according to the guide for the care and use of laboratory animals. Male BALB/c mice (aged 8–10 weeks), purchased from Charles River Laboratories (Beijing, China; license SCXK [Beijing] 2021-0006) and housed in a facility with 12-h light/dark cycles under pathogen-free conditions, were used in all animal experiments. For MenSCs and MenSC-EVs administration, mice were pretreated with LPS (L2880, Sigma, Germany), followed by intratracheal administration of 50 μL MenSCs (1×10^6 cells) or MenSC-EVs (released by 1×10^6 MenSCs over 48 h) after 4-h LPS induction (4 mg/kg, intratracheally [i.t.]). The same volume of PBS was used as a vehicle control, and NHLF-EVs were treated as a negative control of MenSC-EVs group. The lung tissue or BALF was harvested on day 4 post LPS administration. To avoid any influence of the BALF collection procedure on histology features, separate animal experiments were implemented for BALF analysis.

Histological assays

For histological analysis, whole left lungs of mice were fixed in 4% paraformaldehyde, embedded in paraffin, and sectioned at 4 μm. The sections were then subjected to H&E staining and CD68 (GB113109, Servicebio, China) IHC staining. For IHC staining, tissue slides were first baked at 60°C for 2 h, followed by deparaffinization with xylene and rehydration through an ethanol gradient. The slides were then subjected to antigen retrieval by heating at 95°C in citrate buffer (10 mM sodium citrate [pH 6.0]) for 30 min and cooling down to room temperature. After blocking endogenous peroxidase activity and serum sealing, the sections were incubated with appropriate primary and secondary antibodies and then subjected to a DAB chromogenic reaction with a DAB color-developing solution. After nucleus counterstaining and dehydration, images of tissue sections were captured by using an inverted microscope.

RNA extraction and qRT-PCR

Total RNA from right mouse lungs, patient samples, or human cells was extracted for downstream analysis by qRT-PCR and transcriptome sequencing using the RNAsimple Total RNA Kit (DP419, Tiangen, China) according to the manufacturer's instructions. The concentration and purity of the total RNA were evaluated by NanoDrop 2000 (Thermo Scientific, USA). Reverse transcription was performed with 1 μg of total RNA using a 5× All-In-One RT Kit (G486, ABM, Canada). For the reverse transcription of miRNA, a stem-loop-based method was conducted using a RevertAid First Strand cDNA Synthesis Kit (K1622, Thermo Scientific, USA) and normalized to U6 small nuclear RNA (snRNA) for subsequent quantification. All cDNA samples were frozen at −20°C until used. BlasTaq 2X qPCR MasterMix (G891, ABM, Canada) was used for qPCR. The relative changes of mRNA and miRNA were determined by the $2^{-\Delta\Delta Ct}$ method and normalized to glyceraldehyde-3-phosphate dehydrogenase (GAPDH) and U6, respectively. The primer sequences used in the qPCR analysis are shown in Tables S1 and S2.

mRNA sequencing and miRNA microarray chip screening

The mRNA sequencing experiments for MenSCs/MenSC-EVs treatment and AAV-mediated miR-671-5p-depletion in lungs of mice

were performed by Genewiz (Suzhou, China) and Annoroad (Beijing, China), respectively; the detailed experimental procedures and subsequent data analysis were conducted as described previously.[52] The raw data have been deposited in the Sequence Read Archive (SRA) database with BioProject accession number PRJNA872906 (for the MenSCs and MenSC-EVs treatment experiment in lungs of mice) and PRJNA873792 (for the AAV-mediated miR-671-5p depletion experiment in lungs of mice).

miRNA microarray chip screening experiments were performed by OE Biotechnology (Shanghai, China). Total RNA was extracted from MenSC-EVs derived from two different donors and then quantified by Nanodrop 2000 (Thermo Scientific, USA). The RNA integrity number (RIN) was assessed using Agilent Bioanalyzer 2100 (Agilent Technologies, USA). Sample labeling, microarray hybridization, and washing were performed based on the manufacturer's standard protocol. The abundance of miRNAs was normalized with the quantile algorithm. The raw data of the expression profiles for miRNAs derived from MenSC-EVs are shown in Tables S5, S6, and S7 (data accessible at NCBI GEO database, assession GSE223537).

BALF collection and analysis

The lungs of mice were lavaged twice with 600 μL ice-cold PBS to collect BALF, harvested around 1 mL net recovered BALF volume, which was used for WBC counts and, subsequently, acellular content measurements, such as total protein concentration, MPO, and inflammatory factor levels after centrifugation (6,000 rpm, 2 min, 4°C). The total protein level was analyzed with a bicinchoninic acid (BCA) protein assay kit (P0010S) from Beyotime (Shanghai, China), and the concentration of MPO (ab155458, Abcam, UK) and inflammatory factors IL-1β (88-7013-22, Invitrogen, USA) and IL-6 (88-7064-22, Invitrogen, USA) were detected by ELISA following the manufacturer's instructions.

Cell culture and transfection

Two types of epithelial cells, the BEAS-2B cell line and AT2 primary cells, were used for *in vitro* experiments, and HEK293T cells were used for virus packaging. The BEAS-2B (CRL-9609) cell line, isolated from normal human bronchial epithelium, and HEK293T (CRL-3216) cells were purchased from the ATCC and cultured in DMEM (HyClone, USA). The human primary type II alveolar epithelial cells (AT2; HUM-iCELL-a002) were purchased from iCell Bioscience (Shanghai, China) and cultured in DMEM/F12 (HyClone, USA). All culture media were supplemented with 10% FBS (Gibco, USA) and 1% penicillin-streptomycin (Corning, USA). For transfection, HEK293T cells and BEAS-2B/AT2 cells were transfected with the indicated plasmids or *in vitro*-synthesized small interfering RNAs (siRNAs) and the miRNA mimic using LipoFiter 3.0 (HB-TRLF3-1000, HanBio, China) or RNAFit (HB-RF-1000, HanBio, China) according to the manufacturer's instructions.

Plasmid construction and transient and stable RNAi knockdown

FLAG-AAK1 and hemagglutinin (HA)-AAK1 were generated by cloning complementary human DNAs into a pLentivirus-EF1α lentiviral vector. FLAG-p65, FLAG-IκBα, HA-ubiquitin (Ub), and Myc-Ub were generated by cloning complementary human DNAs into a pCMV6 vector. For stable miRNA manipulation or target gene knockdown, a pHBLV-U6 lentiviral vector was used for miRNA depletion, miRNA overexpression, and shRNA expression. Meanwhile, miR-671-5p-sponge and shRNA targeting AAK1 were respectively cloned into a pHBAAV-U6 AAV vector and then used for subsequent depletion of miR-671-5p and AAK1 in the lung tissues of mice. siAAK1 (siG000022848A, RiboBio, China) was purchased for transient target gene silencing to knock down intracellular AAK1. The sequences of RNAi are provided in Tables S3 and S4.

Lentivirus and AAV infection

For lentivirus infection, procedures were conducted as described previously.[53] Briefly, preconstructed pLentivirus-miR-671-5p-sponge, together with PMD2G and PsPaX2 plasmids, were co-transfected into HEK293T cells to produce lentiviral particles, which were ready for MenSCs and BEAS-2B/AT2 cells infection for subsequent *in vivo* and *in vitro* experiments, respectively. For AAV infection, the AAV6 system was used for stably silencing specific factors in the lungs of mice. AAV-based core plasmids depleting the indicated factors, such as miR-671-5p-sponge or shAAK1, together with pAAV-RC6 and pHelper plasmids, were co-transfected into HEK293T cells for production of the AAV. The AAV was extracted 72 h after transfection using an AAVpro Purification Kit (6666, Takara, Japan) according to the manufacturer's instructions. The purified AAV was titrated with an AAVpro Titration Kit (6233, Takara, Japan). After quantification, the AAV (1×10^{12} viral genomes (vg)/mL, 60 μL) was instilled i.t. into the lungs of mice following LPS induction after 3 weeks for further *in vivo* studies, and then all animal samples were harvested 4 days post PBS or LPS stimulation.

Dual-luciferase reporter assay

To detect whether AAK1 is a direct target gene for miR-671-5p, an AAK1 3′ UTR with the normal miR-671-5p-binding site or a Mut binding site was inserted into the psiCHECK-2 reporter vector. The constructed reporter vectors (0.3 μg) were co-transfected with the lentiviral plasmid (1.2 μg) of miR-671-5p or its negative control into HEK293T cells and incubated for 48 h. Subsequently, cells were harvested and lysed, and the luciferase activity was measured with a Dual Luciferase Reporter Gene Assay Kit (RG028, Beyotime, China) following the manufacturer's manual.

Immunoprecipitation and ubiquitination assays

For immunoprecipitation, cells were lysed in a lysis buffer containing 50 mM Tris-HCl (pH 7.4), 150 mM NaCl, 1% Triton X-100, and 1 mM DTT, supplemented with protease and phosphatase inhibitor cocktail. The cell lysates were immunoprecipitated by using anti-DYKDDDDK magnetic beads. The immunoprecipitates were washed four times with the lysis buffer and then subjected to immunoblot analysis. Cells were lysed in a 1% SDS buffer containing Tris-HCl (pH 7.5), 0.5 mM EDTA, 1 mM DTT for the ubiquitination assay. After boiling for 10 min, the cell lysates were diluted 10-fold with Tris-HCl buffer, centrifuged to remove debris, and subjected to

immunoprecipitation with anti-DYKDDDDK magnetic beads. The immunoprecipitates were washed four times with a lysis buffer containing 0.1% SDS and then subjected to immunoblot analysis. The following primary antibodies were used: anti-IκBα (10268-1-AP, Proteintech, China), anti-p65 (10745-1-AP, Proteintech, China), anti-pho-p65 (3033, Cell Signaling Technology, USA), anti-ac-p65 (3045, Cell Signaling Technology, USA), anti-AAK1 (79832, Cell Signaling Technology, USA), anti-GAPDH (2118, Cell Signaling Technology, USA), anti-FLAG (20543-1-AP, Proteintech, China), anti-HA (51064-2-AP, Proteintech, China), and anti-Myc (16286-1-AP, Proteintech, China). Anti-DYKDDDDK magnetic beads (A36798) were purchased from Thermo Fisher Scientific (USA).

EVs uptake experiment

MenSC-EVs were labeled with DiO (C1038, Beyotime, China) at 5 μM final concentration for 15 min, washed in PBS, and then collected by ultracentrifugation (100,000 × *g* for 30 min) at 4°C. Finally, DiO-labeled EVs were resuspended in PBS. Furthermore, DiO-labeled EVs were added to the culture medium of BEAS-2B cells in a confocal dish. After 12 h, cells were fixed with 4% paraformaldehyde after washing three times with PBS, following cell nucleus staining by Hoechst 33342 (B2261, Sigma, USA). Images were obtained using a confocal microscope (SP8, Leica, Germany).

Co-culture assay

After transfection with the miR-671-5p mimic, MenSCs (1×10^5/well) were co-cultured with BEAS-2B cells at a ratio of 1:1 using a Transwell plate (0.4 μm, Corning, USA) for 12 h, with BEAS-2B cells placed in the lower chamber and MenSCs placed in the upper chamber. MenSCs treated with mimic-NC were used in the control group. To inhibit EVs secretion, MenSCs mimics were pretreated with GW4869 (6823-69-4, Selleck, China), an inhibitor of neutral sphingomyelinase, at 10 μM for 24 h.[22,54] These MenSCs were used for co-culture with BEAS-2B cells in medium containing GW4869 for another 12 h.

Patient samples

Lung specimens from the patients with organizing pneumonia were obtained following research ethics board approval from Xinxiang Medical University. As described above, samples isolated from lesion areas and corresponding adjacent normal areas were subjected to quantitative PCR analysis and FISH staining. The detailed clinical information of patients is shown in Table S8.

FISH assay

Briefly, the fixed paraffin-embedded lung tissue sections were first baked at 60°C for 2 h, followed by deparaffinization in xylene and rehydration through graded series of ethanol. After tissue permeabilization within proteinase K (20 μg/mL) working solution, the slides were subjected to hybridization using an antisense probe against has-miR-671-5p labeled with Cy3 at a concentration of 500 nM in hybridization buffer and incubated at 42°C overnight, then incubated in the signal probe hybridization solution at 40°C overnight for signal amplification, followed by a rinse in 2× saline sodium citrate (SSC) at 40°C. After nucleus counterstaining with DAPI, the tissue slides were mounted for microscopic examination and photography. The probe used in the FISH assay is shown in Table S9.

Statistical analysis

All statistical analysis was performed using GraphPad Prism 9. Briefly, t tests and one-way ANOVA were used to compare two groups and multiple groups. The distribution of all data was tested for normality via a Shapiro-Wilk test, and a parametric or nonparametric test was used for subsequent statistical analysis based on whether the data were normally distributed or not. Data are presented as mean ± SD. A Student's t test was used for comparisons to compare two groups with normal distribution, while a Mann-Whitney test was used to compare ranks when the data did not follow a normal distribution. For comparison among multiple groups with normal distribution, data were analyzed by Brown-Forsythe and Welch ANOVA tests following Tukey's or Dunnett's T3 post hoc test, whereas a Kruskal-Wallis test with Dunn's post hoc correction was used for multiple comparisons with non-normally distributed variables. A p value of less than 0.05 was considered statistically significant. In the figure legends, n refers to the number of samples or mice, not the number of replicate experiments for the same sample or mouse.

DATA AVAILABILITY

The raw data of high-throughput mRNA sequencing analysis have been deposited into the SRA database, produced by the National Center for Biotechnology Information (NCBI) at the National Institutes of Health (NIH), with BioProject accession numbers PRJNA872906 and PRJNA873792. The raw data of microRNA mricroarray analysis of MenSC-EVs have been deposited into NCBI's GEO database and are accessible through GEO Series accession number GSE223537.

SUPPLEMENTAL INFORMATION

Supplemental information can be found online at https://doi.org/10.1016/j.ymthe.2023.01.025.

ACKNOWLEDGMENTS

This work was supported by grants from the National Natural Science Foundation of China (81900392 to X.Z.), the Natural Science Foundation of Henan Province for Distinguished Young Scholars (202300410307 to J. Lin), and the Ministry of Higher Education Malaysia for the Fundamental Research Grant Scheme (FRGS/1/2019/STG03/USM/02/2 to B.Y.). The graphical abstract and Figures 6A, S1A, and S2A were created under the academic license of BioRender.

AUTHOR CONTRIBUTIONS

J. Lin, J. Lian, and X.Z. designed and conceived the project. J. Lian and X.Z. performed most of the experiments, analyzed data, and wrote the manuscript. B.H. and J.D. collected clinical samples and conducted the subsequent analysis. F.Z. and C.M. established the animal models and collected animal samples. R.G. collected EVs and the subsequent microarray chip analysis. Y.Z. and L.J. performed cDNA cloning and shRNA preparation. J. Lin, B.Y., and X.Z. supervised the work and

revised the manuscript. All authors gave final approval of the manuscript.

DECLARATION OF INTERESTS

The authors declare no competing interests.

REFERENCES

1. Lian, J., Lin, J., Zakaria, N., and Yahaya, B.H. (2020). Acute lung injury: disease modelling and the therapeutic potential of stem cells. Adv. Exp. Med. Biol. *1298*, 149–166. https://doi.org/10.1007/5584_2020_538.
2. Huang, C., Wang, Y., Li, X., Ren, L., Zhao, J., Hu, Y., Zhang, L., Fan, G., Xu, J., Gu, X., et al. (2020). Clinical features of patients infected with 2019 novel coronavirus in Wuhan, China. Lancet *395*, 497–506. https://doi.org/10.1016/S0140-6736(20)30183-5.
3. Tzotzos, S.J., Fischer, B., Fischer, H., and Zeitlinger, M. (2020). Incidence of ARDS and outcomes in hospitalized patients with COVID-19: a global literature survey. Crit. Care *24*, 516. https://doi.org/10.1186/s13054-020-03240-7.
4. Xu, Z., Shi, L., Wang, Y., Zhang, J., Huang, L., Zhang, C., Liu, S., Zhao, P., Liu, H., Zhu, L., et al. (2020). Pathological findings of COVID-19 associated with acute respiratory distress syndrome. Lancet Respir. Med. *8*, 420–422. https://doi.org/10.1016/S2213-2600(20)30076-X.
5. Galipeau, J., and Sensébé, L. (2018). Mesenchymal stromal cells: clinical challenges and therapeutic opportunities. Cell Stem Cell *22*, 824–833. https://doi.org/10.1016/j.stem.2018.05.004.
6. Qu, W., Wang, Z., Hare, J.M., Bu, G., Mallea, J.M., Pascual, J.M., Caplan, A.I., Kurtzberg, J., Zubair, A.C., Kubrova, E., et al. (2020). Cell-based therapy to reduce mortality from COVID-19: systematic review and meta-analysis of human studies on acute respiratory distress syndrome. Stem Cells Transl. Med. *9*, 1007–1022. https://doi.org/10.1002/sctm.20-0146.
7. Qin, H., and Zhao, A. (2020). Mesenchymal stem cell therapy for acute respiratory distress syndrome: from basic to clinics. Protein Cell *11*, 707–722. https://doi.org/10.1007/s13238-020-00738-2.
8. Khoury, M., Cuenca, J., Cruz, F.F., Figueroa, F.E., Rocco, P.R.M., and Weiss, D.J. (2020). Current status of cell-based therapies for respiratory virus infections: applicability to COVID-19. Eur. Respir. J. *55*, 2000858. https://doi.org/10.1183/13993003.00858-2020.
9. Xu, X., Jiang, W., Chen, L., Xu, Z., Zhang, Q., Zhu, M., Ye, P., Li, H., Yu, L., Zhou, X., et al. (2021). Evaluation of the safety and efficacy of using human menstrual blood-derived mesenchymal stromal cells in treating severe and critically ill COVID-19 patients: an exploratory clinical trial. Clin. Transl. Med. *11*, e297. https://doi.org/10.1002/ctm2.297.
10. Askenase, P.W. (2020). COVID-19 therapy with mesenchymal stromal cells (MSC) and convalescent plasma must consider exosome involvement: do the exosomes in convalescent plasma antagonize the weak immune antibodies? J. Extracell. Vesicles *10*, e12004. https://doi.org/10.1002/jev2.12004.
11. Abdelgawad, M., Bakry, N.S., Farghali, A.A., Abdel-Latif, A., and Lotfy, A. (2021). Mesenchymal stem cell-based therapy and exosomes in COVID-19: current trends and prospects. Stem Cell Res. Ther. *12*, 469. https://doi.org/10.1186/s13287-021-02542-z.
12. Chrzanowski, W., Kim, S.Y., and McClements, L. (2020). Can stem cells beat COVID-19: advancing stem cells and extracellular vesicles toward mainstream medicine for lung injuries associated with SARS-CoV-2 infections. Front. Bioeng. Biotechnol. *8*, 554. https://doi.org/10.3389/fbioe.2020.00554.
13. EL Andaloussi, S., Mäger, I., Breakefield, X.O., and Wood, M.J.A. (2013). Extracellular vesicles: biology and emerging therapeutic opportunities. Nat. Rev. Drug Discov. *12*, 347–357. https://doi.org/10.1038/nrd3978.
14. Herrmann, I.K., Wood, M.J.A., and Fuhrmann, G. (2021). Extracellular vesicles as a next-generation drug delivery platform. Nat. Nanotechnol. *16*, 748–759. https://doi.org/10.1038/s41565-021-00931-2.
15. Liu, H., Lei, C., He, Q., Pan, Z., Xiao, D., and Tao, Y. (2018). Nuclear functions of mammalian MicroRNAs in gene regulation, immunity and cancer. Mol. Cancer *17*, 64. https://doi.org/10.1186/s12943-018-0765-5.
16. Feng, Z., Qi, S., Zhang, Y., Qi, Z., Yan, L., Zhou, J., He, F., Li, Q., Yang, Y., Chen, Q., et al. (2017). Ly6G+ neutrophil-derived miR-223 inhibits the NLRP3 inflammasome in mitochondrial DAMP-induced acute lung injury. Cell Death Dis. *8*, e3170. https://doi.org/10.1038/cddis.2017.549.
17. Neudecker, V., Brodsky, K.S., Clambey, E.T., Schmidt, E.P., Packard, T.A., Davenport, B., Standiford, T.J., Weng, T., Fletcher, A.A., Barthel, L., et al. (2017). Neutrophil transfer of miR-223 to lung epithelial cells dampens acute lung injury in mice. Sci. Transl. Med. *9*, eaah5360. https://doi.org/10.1126/scitranslmed.aah5360.
18. Smith, S., Wu, P.W., Seo, J.J., Fernando, T., Jin, M., Contreras, J., Montano, E.N., Gabhann, J.N., Cunningham, K., Widaa, A., et al. (2018). IL-16/miR-125a axis controls neutrophil recruitment in pristane-induced lung inflammation. JCI Insight *3*, e120798. https://doi.org/10.1172/jci.insight.120798.
19. Yang, B., Schwartz, M., and McJunkin, K. (2020). In vivo CRISPR screening for phenotypic targets of the mir-35-42 family in C. elegans. Genes Dev. *34*, 1227–1238. https://doi.org/10.1101/gad.339333.120.
20. Tran, A.T., Chapman, E.M., Flamand, M.N., Yu, B., Krempel, S.J., Duchaine, T.F., Eroglu, M., and Derry, W.B. (2019). MiR-35 buffers apoptosis thresholds in the C. elegans germline by antagonizing both MAPK and core apoptosis pathways. Cell Death Differ. *26*, 2637–2651. https://doi.org/10.1038/s41418-019-0325-6.
21. Nucera, S., Giustacchini, A., Boccalatte, F., Calabria, A., Fanciullo, C., Plati, T., Ranghetti, A., Garcia-Manteiga, J., Cittaro, D., Benedicenti, F., et al. (2016). miRNA-126 orchestrates an oncogenic program in B cell precursor acute lymphoblastic leukemia. Cancer Cell *29*, 905–921. https://doi.org/10.1016/j.ccell.2016.05.007.
22. Ying, W., Riopel, M., Bandyopadhyay, G., Dong, Y., Birmingham, A., Seo, J.B., Ofrecio, J.M., Wollam, J., Hernandez-Carretero, A., Fu, W., et al. (2017). Adipose tissue macrophage-derived exosomal miRNAs can modulate in vivo and in vitro insulin sensitivity. Cell *171*, 372–384.e12. https://doi.org/10.1016/j.cell.2017.08.035.
23. Zhao, J., Li, X., Hu, J., Chen, F., Qiao, S., Sun, X., Gao, L., Xie, J., and Xu, B. (2019). Mesenchymal stromal cell-derived exosomes attenuate myocardial ischaemia-reperfusion injury through miR-182-regulated macrophage polarization. Cardiovasc. Res. *115*, 1205–1216. https://doi.org/10.1093/cvr/cvz040.
24. Wang, C., Wang, J., Shuai, L., Ma, X., Zhang, H., Liu, R., Chen, W., Wang, X., Ge, J., Wen, Z., and Bu, Z. (2019). The serine/threonine kinase AP2-associated kinase 1 plays an important role in rabies virus entry. Viruses *12*, 45. https://doi.org/10.3390/v12010045.
25. Bekerman, E., Neveu, G., Shulla, A., Brannan, J., Pu, S.Y., Wang, S., Xiao, F., Barouch-Bentov, R., Bakken, R.R., Mateo, R., et al. (2017). Anticancer kinase inhibitors impair intracellular viral trafficking and exert broad-spectrum antiviral effects. J. Clin. Invest. *127*, 1338–1352. https://doi.org/10.1172/jci89857.
26. Hyder Pottoo, F., Abu-Izneid, T., Mohammad Ibrahim, A., Noushad Javed, M., AlHajri, N., and Hamrouni, A.M. (2021). Immune system response during viral Infections: immunomodulators, cytokine storm (CS) and Immunotherapeutics in COVID-19. Saudi Pharm. J. *29*, 173–187. https://doi.org/10.1016/j.jsps.2020.12.018.
27. Tang, B., Zhu, J., Cong, Y., Yang, W., Kong, C., Chen, W., Wang, Y., Zeng, Y., and Ji, J. (2020). The landscape of coronavirus disease 2019 (COVID-19) and integrated analysis SARS-CoV-2 receptors and potential inhibitors in lung adenocarcinoma patients. Front. Cell Dev. Biol. *8*, 577032. https://doi.org/10.3389/fcell.2020.577032.
28. Richardson, P., Griffin, I., Tucker, C., Smith, D., Oechsle, O., Phelan, A., Rawling, M., Savory, E., and Stebbing, J. (2020). Baricitinib as potential treatment for 2019-nCoV acute respiratory disease. Lancet *395*, e30–e31. https://doi.org/10.1016/s0140-6736(20)30304-4.
29. Esteves, M., Abreu, R., Fernandes, H., Serra-Almeida, C., Martins, P.A.T., Barão, M., Cristóvão, A.C., Saraiva, C., Ferreira, R., Ferreira, L., and Bernardino, L. (2022). MicroRNA-124-3p-enriched small extracellular vesicles as a therapeutic approach for Parkinson's disease. Mol. Ther. *30*, 3176–3192. https://doi.org/10.1016/j.ymthe.2022.06.003.
30. Yu, Z., Wen, Y., Jiang, N., Li, Z., Guan, J., Zhang, Y., Deng, C., Zhao, L., Zheng, S.G., Zhu, Y., et al. (2022). TNF-α stimulation enhances the neuroprotective effects of gingival MSCs derived exosomes in retinal ischemia-reperfusion injury via the MEG3/miR-21a-5p axis. Biomaterials *284*, 121484. https://doi.org/10.1016/j.biomaterials.2022.121484.
31. Wang, J., Huang, R., Xu, Q., Zheng, G., Qiu, G., Ge, M., Shu, Q., and Xu, J. (2020). Mesenchymal stem cell-derived extracellular vesicles alleviate acute lung injury via

transfer of miR-27a-3p. Crit. Care Med. *48*, e599–e610. https://doi.org/10.1097/CCM.0000000000004315.

32. Monsel, A., Zhu, Y.G., Gennai, S., Hao, Q., Hu, S., Rouby, J.J., Rosenzwajg, M., Matthay, M.A., and Lee, J.W. (2015). Therapeutic effects of human mesenchymal stem cell-derived microvesicles in severe pneumonia in mice. Am. J. Respir. Crit. Care Med. *192*, 324–336. https://doi.org/10.1164/rccm.201410-1765OC.

33. Rani, S., Ryan, A.E., Griffin, M.D., and Ritter, T. (2015). Mesenchymal stem cell-derived extracellular vesicles: toward cell-free therapeutic applications. Mol. Ther. *23*, 812–823.

34. Théry, C., Witwer, K.W., Aikawa, E., Alcaraz, M.J., Anderson, J.D., Andriantsitohaina, R., Antoniou, A., Arab, T., Archer, F., Atkin-Smith, G.K., et al. (2018). Minimal information for studies of extracellular vesicles 2018 (MISEV2018): a position statement of the International Society for Extracellular Vesicles and update of the MISEV2014 guidelines. J. Extracell. Vesicles *7*, 1535750.

35. Ferruelo, A., Peñuelas, Ó., and Lorente, J.A. (2018). MicroRNAs as biomarkers of acute lung injury. Ann. Transl. Med. *6*, 34. https://doi.org/10.21037/atm.2018.01.10.

36. Bobba, C.M., Fei, Q., Shukla, V., Lee, H., Patel, P., Putman, R.K., Spitzer, C., Tsai, M., Wewers, M.D., Lee, R.J., et al. (2021). Nanoparticle delivery of microRNA-146a regulates mechanotransduction in lung macrophages and mitigates injury during mechanical ventilation. Nat. Commun. *12*, 289. https://doi.org/10.1038/s41467-020-20449-w.

37. Ebert, M.S., Neilson, J.R., and Sharp, P.A. (2007). MicroRNA sponges: competitive inhibitors of small RNAs in mammalian cells. Nat. Methods *4*, 721–726. https://doi.org/10.1038/nmeth1079.

38. Wang, X., Liu, D., Zhang, X., Yang, L., Xia, Z., and Zhang, Q. (2022). Exosomes from adipose-derived mesenchymal stem cells alleviate sepsis-induced lung injury in mice by inhibiting the secretion of IL-27 in macrophages. Cell Death Discov. *8*, 18. https://doi.org/10.1038/s41420-021-00785-6.

39. Moradinasab, S., Pourbagheri-Sigaroodi, A., Zafari, P., Ghaffari, S.H., and Bashash, D. (2021). Mesenchymal stromal/stem cells (MSCs) and MSC-derived extracellular vesicles in COVID-19-induced ARDS: mechanisms of action, research progress, challenges, and opportunities. Int. Immunopharmacol. *97*, 107694. https://doi.org/10.1016/j.intimp.2021.107694.

40. Torres Acosta, M.A., and Singer, B.D. (2020). Pathogenesis of COVID-19-induced ARDS: implications for an ageing population. Eur. Respir. J. *56*, 2002049. https://doi.org/10.1183/13993003.02049-2020.

41. Maggi, E., Canonica, G.W., and Moretta, L. (2020). COVID-19: unanswered questions on immune response and pathogenesis. J. Allergy Clin. Immunol. *146*, 18–22. https://doi.org/10.1016/j.jaci.2020.05.001.

42. Zhao, S., Mi, Y., Zheng, B., Wei, P., Gu, Y., Zhang, Z., Xu, Y., Cai, S., Li, X., and Li, D. (2022). Highly-metastatic colorectal cancer cell released miR-181a-5p-rich extracellular vesicles promote liver metastasis by activating hepatic stellate cells and remodelling the tumour microenvironment. J. Extracell. Vesicles *11*, e12186. https://doi.org/10.1002/jev2.12186.

43. Cao, M., Isaac, R., Yan, W., Ruan, X., Jiang, L., Wan, Y., Wang, J., Wang, E., Caron, C., Neben, S., et al. (2022). Cancer-cell-secreted extracellular vesicles suppress insulin secretion through miR-122 to impair systemic glucose homeostasis and contribute to tumour growth. Nat. Cell Biol. *24*, 954–967. https://doi.org/10.1038/s41556-022-00919-7.

44. He, Y., Rodrigues, R.M., Wang, X., Seo, W., Ma, J., Hwang, S., Fu, Y., Trojnár, E., Mátyás, C., Zhao, S., et al. (2021). Neutrophil-to-hepatocyte communication via LDLR-dependent miR-223-enriched extracellular vesicle transfer ameliorates nonalcoholic steatohepatitis. J. Clin. Invest. *131*, e141513. https://doi.org/10.1172/jci141513.

45. Ge, L., Xun, C., Li, W., Jin, S., Liu, Z., Zhuo, Y., Duan, D., Hu, Z., Chen, P., and Lu, M. (2021). Extracellular vesicles derived from hypoxia-preconditioned olfactory mucosa mesenchymal stem cells enhance angiogenesis via miR-612. J. Nanobiotechnology *19*, 380. https://doi.org/10.1186/s12951-021-01126-6.

46. Ding, J., Zhang, Y., Cai, X., Zhang, Y., Yan, S., Wang, J., Zhang, S., Yin, T., Yang, C., and Yang, J. (2021). Extracellular vesicles derived from M1 macrophages deliver miR-146a-5p and miR-146b-5p to suppress trophoblast migration and invasion by targeting TRAF6 in recurrent spontaneous abortion. Theranostics *11*, 5813–5830. https://doi.org/10.7150/thno.58731.

47. Ren, W., Hou, J., Yang, C., Wang, H., Wu, S., Wu, Y., Zhao, X., and Lu, C. (2019). Extracellular vesicles secreted by hypoxia pre-challenged mesenchymal stem cells promote non-small cell lung cancer cell growth and mobility as well as macrophage M2 polarization via miR-21-5p delivery. J. Exp. Clin. Cancer Res. *38*, 62. https://doi.org/10.1186/s13046-019-1027-0.

48. Lien, G.-S., Liu, J.-F., Chien, M.-H., Hsu, W.-T., Chang, T.-H., Ku, C.-C., Ji, A.T.-Q., Tan, P., Hsieh, T.-L., Lee, L.-M., and Ho, J.H. (2014). The ability to suppress macrophage-mediated inflammation in orbital fat stem cells is controlled by miR-671-5p. Stem Cell Res. Ther. *5*, 97. https://doi.org/10.1186/scrt486.

49. Zhang, W., Zhao, Y., Zhang, F., Wang, Q., Li, T., Liu, Z., Wang, J., Qin, Y., Zhang, X., Yan, X., et al. (2020). The use of anti-inflammatory drugs in the treatment of people with severe coronavirus disease 2019 (COVID-19): the Perspectives of clinical immunologists from China. Clin. Immunol. *214*, 108393. https://doi.org/10.1016/j.clim.2020.108393.

50. Agajanian, M.J., Walker, M.P., Axtman, A.D., Ruela-de-Sousa, R.R., Serafin, D.S., Rabinowitz, A.D., Graham, D.M., Ryan, M.B., Tamir, T., Nakamichi, Y., et al. (2019). WNT activates the AAK1 kinase to promote clathrin-mediated endocytosis of LRP6 and establish a negative feedback loop. Cell Rep. *26*, 79–93.e8. https://doi.org/10.1016/j.celrep.2018.12.023.

51. Ridzuan, N., Zakaria, N., Widera, D., Sheard, J., Morimoto, M., Kiyokawa, H., Mohd Isa, S.A., Chatar Singh, G.K., Then, K.Y., Ooi, G.C., and Yahaya, B.H. (2021). Human umbilical cord mesenchymal stem cell-derived extracellular vesicles ameliorate airway inflammation in a rat model of chronic obstructive pulmonary disease (COPD). Stem Cell Res. Ther. *12*, 54. https://doi.org/10.1186/s13287-020-02088-6.

52. Zhu, X., Liu, Y., Yu, J., Du, J., Guo, R., Feng, Y., Zhong, G., Jiang, Y., and Lin, J. (2019). LncRNA HOXA-AS2 represses endothelium inflammation by regulating the activity of NF-kappaB signaling. Atherosclerosis *281*, 38–46. https://doi.org/10.1016/j.atherosclerosis.2018.12.012.

53. Zhu, X., Du, J., Yu, J., Guo, R., Feng, Y., Qiao, L., Xu, Z., Yang, F., Zhong, G., Liu, F., et al. (2019). LncRNA NKILA regulates endothelium inflammation by controlling a NF-kappaB/KLF4 positive feedback loop. J. Mol. Cell. Cardiol. *126*, 60–69. https://doi.org/10.1016/j.yjmcc.2018.11.001.

54. Kosaka, N., Iguchi, H., Yoshioka, Y., Takeshita, F., Matsuki, Y., and Ochiya, T. (2010). Secretory mechanisms and intercellular transfer of microRNAs in living cells. J. Biol. Chem. *285*, 17442–17452. https://doi.org/10.1074/jbc.M110.107821.